Check for updates

Dual-network low-methoxyl amidated pectin–protein films: mechanism, optimization, and application to fresh foods

Y. Doan Trang Tran,[a] Thi Thao Minh,[b] Dinh Nhi Bui [ID] *[c] and Thi Dung Ha[d]

This study reports an edible-film platform that valorizes Hàm Yên orange peel low-methoxyl amidated pectin (LM/LMA) and bee brood protein (BBP, *Apis mellifera*) through dual structuring: complex coacervation between pectin(−) and BBP(+) at pH 4.7, and Ca^{2+} "egg-box" crosslinking of homogalacturonan junctions. BBP was obtained *via* defatting → mild alkaline extraction → isoelectric precipitation; LM/LMA pectin was prepared from local citrus peel and plasticized with glycerol. A design–make–measure loop combined turbidity/ζ-potential/DLS maps to locate the coacervation window, and then tuned casting and post-$CaCl_2$ treatment. Under the optimized recipe (LMA 2.5% w/v; BBP 0.5% w/v; glycerol 25% on polymer; $CaCl_2$ 1.5% w/v; pH 4.7), the hybrid film achieved a balanced property set: tensile strength (TS) $\approx$ 51 MPa, elongation at break (EAB) $\approx$ 20.5%, storage elastic tissue E' (DMA E') $\approx$ 1.18 GPa, water vapor permeability (WVP) $\approx$ 4.6 g mm per m^2 per day per kPa, oxygen transmission rate (OTR) $\approx$ 60 cm^3 per m^2 per day, glass transition temperature (T_g) $\approx$ 54 °C, T_{600} $\approx$ 80%, haze $\approx$ 14%, contact angle $\approx$ 71°. FTIR resolved amide–COO^- electrostatic pairing and Ca–pectinate signatures; SEM revealed a compact, defect-poor cross-section; TGA/DSC showed multi-step dehydration/plasticizer loss and polysaccharide degradation typical of Ca^{2+}-reinforced pectin networks. Safety profiling met food-contact expectations (Pb/Cd/As/Hg at trace levels; total plate count (TPC) and yeast–mold <10 CFU g^{-1}; *E. coli*, *Salmonella*, *S. aureus* not detected) and the film disintegrated to ~18% mass remaining at day 60 under lab composting. In pilot applications, coatings on beef (4 °C) and tomato (12 °C) slowed drip/weight loss, lipid oxidation (TBARS), texture softening, pH drift, microbial growth, and decay incidence *versus* pectin-only and control, indicating effective moisture/oxygen moderation and surface conditioning by the pectin–protein–Ca^{2+} network. The results demonstrate a circular, locally sourced, protein–polysaccharide film that reconciles mechanical robustness, gas/water-vapor resistance, optics, safety, and biodegradability, with clear translational potential for fresh-food preservation.

Sustainability spotlight

This work advances circular food-packaging solutions by converting two underutilized local biomasses, Hàm Yên orange-peel low-methoxyl amidated pectin and honeybee brood protein, into a high-performance edible film. Through pH-tuned protein–pectin complexation and Ca^{2+} "egg-box" reinforcement, the film achieves a robust balance of strength, barrier properties, and optics while remaining food-contact safe (trace metals and no detected pathogens). Importantly, it shows rapid compost disintegration with ~18% mass remaining after 60 days, supporting end-of-life sustainability compared with conventional plastics. In pilot trials, coatings on beef (4 °C) and tomatoes (12 °C) slowed quality loss and microbial/oxidative spoilage, indicating potential to reduce food waste alongside plastic reduction.

1 Introduction

Amid mounting pressure to replace non-biodegradable plastics, biopolymer based edible films are gaining attention as sustainable packaging alternatives. Pectin, especially when recovered from citrus peel by products, is a safe and abundant film forming polysaccharide that can form a tunable gel network (junction zones whose crosslink density can be adjusted *via* pectin esterification/amidation level, pH, and Ca^{2+} concentration). In parallel, insect derived proteins such as honeybee brood provide a sustainable protein source and enable polysaccharide protein hybrids in which electrostatic interactions and additional bonding can enhance film integrity and moisture resistance beyond pectin alone. Together, these

[a]*Institute of Technology – HaUI, Hanoi University of Industry, Vietnam*
[b]*Faculty of New Energy, Electric Power University, Hanoi, Vietnam*
[c]*Faculty of Natural Sciences, Electric Power University, Hanoi, Vietnam*
[d]*Faculty Chemical Technology, Hanoi University of Industry, 298 Cau Dien, Tay Tuu, Hanoi, 11900, Vietnam. E-mail: nhibd@epu.edu.vn*

drivers motivate the present work, which combines orange peel pectin and bee brood pupa protein to develop edible films aligned with a circular economy approach.[1,2] In terms of supply, the global citrus industry generates large volumes of peel, fiber, and seed by products after juicing, creating an abundant pectin rich resource. Annual citrus production is commonly reported at roughly 100 to 150 million tons, and industrial processing produces several million tons of residues each year, with peel representing the largest and most pectin concentrated fraction. Recovering pectin from these streams is therefore attractive not only for its technical potential, but also for reducing waste related environmental burdens, improving resource efficiency, and increasing value across the citrus supply chain in accordance with circular bioeconomy principles (*i.e.*, valorizing agro-industrial by-products into renewable materials while reducing waste and closing resource loops).[2–7]

Pectins are a family of galacturonic acid based polysaccharides with diverse architectures. In food technology, they are commonly classified by degree of methoxylation. High methoxyl pectin with a degree of esterification above 50 percent forms gels under acidic conditions and at high soluble solids, typically in the presence of sucrose. In contrast, low methoxyl pectin with a degree of esterification at or below 50 percent and low methoxyl amidated pectin form gels through calcium mediated junction zones that follow the egg box model. Calcium binding along the homogalacturonan segments enables low methoxyl pectin (LM) and low methoxyl amidated pectin (LMA) to form strong networks at relatively low solids and under neutral to slightly acidic conditions, which is advantageous for edible film formation.[8] In addition, amidated LM pectin often achieves gelation at lower calcium levels than non-amidated LM, offering greater formulation flexibility.[9] Industrial extraction of pectin from orange and lemon peels typically relies on hot acid extraction followed by alcohol precipitation, washing, and drying. Extraction conditions including acid type, pH, and the temperature and time profile strongly influence both yield and key quality attributes such as degree of esterification or methoxylation, galacturonic acid content, and solution viscosity. To improve sustainability and preserve polymer integrity, recent work increasingly explores greener process intensification using organic acids and energy efficient assistance methods such as ultrasound or microwave treatment. For film and coating applications, commercial citrus derived LM and LMA pectins are often selected to ensure batch to batch reproducibility, yet pectin recovered from locally available peel by products remains a viable option when extraction conditions are carefully controlled, as demonstrated in multiple studies.[10–13]

Low methoxyl amidated pectin is particularly suitable for calcium reinforced cast films. It is typically produced by de-esterifying pectin and then partially amidating a portion of the carboxyl groups with ammonia under controlled alcoholic and alkaline conditions to minimize chain degradation. This modification generally yields a pectin that gels more readily and can achieve comparable network strength at lower calcium levels than non-amidated low methoxyl pectin. Academic studies and technological descriptions, including patents and manufacturer technical documents, consistently support this mechanism. In addition, regulatory assessments by EFSA and JECFA consider pectin and amidated pectin to be safe for the general population when used as food additives according to good manufacturing practice, while noting specific considerations for infants younger than 16 weeks.[14,15] At the material level, pure pectin films offer many advantages (transparency, good O_2 barrier), but are less hydrophobic and brittle if not plasticized. Studies have shown that glycerol/sorbitol are common plasticizers that increase ductility and elongation at break; however, excessive plasticization reduces tensile strength and increases moisture permeability. Another strategy for improving mechanical properties and moisture barrier properties is post-molding exogenous Ca^{2+} treatment: with LM/LMA pectin, increased Ca^{2+} concentration reduces WVP (water vapor permeability), increases modulus, and improves thermal stability, although optimization is needed to avoid over-plasticization that causes brittleness or reduced transparency. Pectin is also a convenient base to carry active ingredients (polyphenols, essential oils), creating an active antioxidant/antibacterial film, suitable for packaging fresh foods.[16,17] To go further, the approach of combining pectin with protein has proven effective in many model systems (whey, pea, caseinate…), inspired by the protein–polysaccharide complex coacervation phenomenon (liquid–liquid phase separation driven by electrostatic attraction between oppositely charged biopolymers, yielding a dense polymer-rich coacervate): when the pH of the mixture is set just below the isoelectric point (pI) of the protein, the positively charged protein charges pair with the negatively charged pectin to form a homogeneous polymer-rich phase, thereby forming a film with a dense hydrogen/ion bond network. The methoxyl level of pectin, the free carboxyl order, the coupling ratio, and the ionic strength are all variables that control the size–stability of the complex, thus, choosing pectin LM/LMA and setting the pH at 4.5–5.0 is a promising window when combining with easily protonated proteins. Mechanistic framework and quantitative data on optimal pH, complex particle size, and application to pectin – whey nanoparticles/films have been well summarized in the literature.[18–21] The choice of key parameters (mixture pH, post-casting $CaCl_2$ concentration, protein/pectin ratio, and glycerol dose) can be based on experience from whey – pectin model systems and pectin–Ca investigations, while also being open to optimizing surface reactions (*e.g.* tannic acid or genipin at very low doses) to lock amino groups and increase moisture resistance when needed.[22,23]

Meanwhile, honeybee brood, an insect biomass of increasing interest, has been characterized as rich in proteins with lipids, minerals, and vitamins; recent reviews confirm the nutritional and food potential of bee brood, while calling for safety standards for its inclusion in products. Regarding separation technologies, established protocols for insect proteins are based on alkaline extraction and isoelectric precipitation, with assisted (ultrasonic) variations to increase yield and solubility. Evidence from the application of insect protein-based film materials, particularly silkworm pupa protein films coated with cheese, or cricket matrix films with enhanced microbial-oxidation

stability, provides valuable precedents for protein phase replacement with bee pupa protein in pectin–protein film systems.[24–27] One caveat is the allergenic risk associated with insect proteins. The immuno-allergy review shows the possibility of cross-reactivity with crustacean-house dust mite allergens (tropomyosin, arginine kinase…), implying the need for risk assessment and appropriate labelling in products containing insect proteins. This is a factor that does not negate the research direction of film materials, but forms a safety framework when evaluating food contact applications.[28,29]

Building on this background, combining orange peel pectin, preferably LM or LMA, with bee pupa protein offers a clear rationale for developing edible films. LM and LMA pectin provide an anionic matrix that can be strengthened by calcium mediated junction zones, improving mechanical integrity and reducing water vapor permeability. Bee pupa protein can further participate in the network through hydrogen bonding and electrostatic interactions, and pH controlled association can promote a more uniform microstructure and enhance tensile performance at an appropriate dosage. This hybrid platform is also compatible with incorporating citrus derived bioactive compounds such as flavonoids or essential oils, enabling functional films with added antioxidant and antibacterial potential.[16,30–34] Importantly, the approach valorizes locally available by products from citrus processing and beekeeping biomass, supporting circularity and reduced environmental burdens.

This study therefore aims to design, fabricate and characterize bee pupa pectin–protein films with key variables (pH distribution just below the protein pI; 1–2% CaCl$_2$ post-casting; 20–30% glycerol; protein content 0.1–0.7% w/v) based on evidence of co-agglomeration and Ca^{2+} gelation (Fig. 1), and to evaluate the physical–mechanical system, water vapor permeability, microstructure and potential for model packaging applications (*e.g.*, fresh fruits and vegetables). This roadmap

hopes to provide a two-in-one edible film material model: both optimizing performance and realizing the circular economy vision for the citrus and beekeeping industries.

2 Experimental

2.1. Orange peel pectin (LMA)

Pectin was prepared from Ham Yen orange peel (Tuyen Quang, Vietnam) collected after juice pressing. The peel was immediately refrigerated and processed within 24 h under general hygienic/food-grade handling conditions, including clean work surfaces, cleaned and sanitized utensils/containers, use of gloves, masks, and hair covers by operators, and prevention of cross-contamination. The procedure is described as follows:

(1) Raw material pre-treatment: orange peel was washed under running water, blanched at 80–90 °C for 1–2 min to inactivate endogenous enzymes, air-dried at 50–55 °C to a moisture content of approximately 10–12%, and ground to a particle size ≤0.5 mm. When deodorization and pigment removal were required, the ground peel was washed with hot ethanol (70 °C) at a peel : ethanol ratio of 1 : 10 (w/v) for 20 min and then re-dried prior to extraction.

(2) Acid extraction and recovery of crude pectin: pectin was extracted in distilled water acidified with citric acid and adjusted to pH 1.6–1.8. The mixture was stirred at 85–90 °C for 60–90 min using a solid-to-liquid ratio of 1 : 15–1 : 20 (w/v). After centrifugation, the pectin-containing supernatant was decolorized with activated carbon (0.3%, 10 min) and adjusted to pH 3.0. Pectin was precipitated by adding 70% (v/v) ethanol at an extract : ethanol ratio of at least 1 : 1, mixed for 30 min, and allowed to stand for 60 min. The precipitate was collected by centrifugation, washed with ethanol 2–3 times to a light cream color, dried at 50 °C, and milled to obtain crude pectin.[10,11,35]

(3) Preparation of LM-pectin (DE ≤ 50%): crude pectin from the same batch was subjected to controlled de-esterification
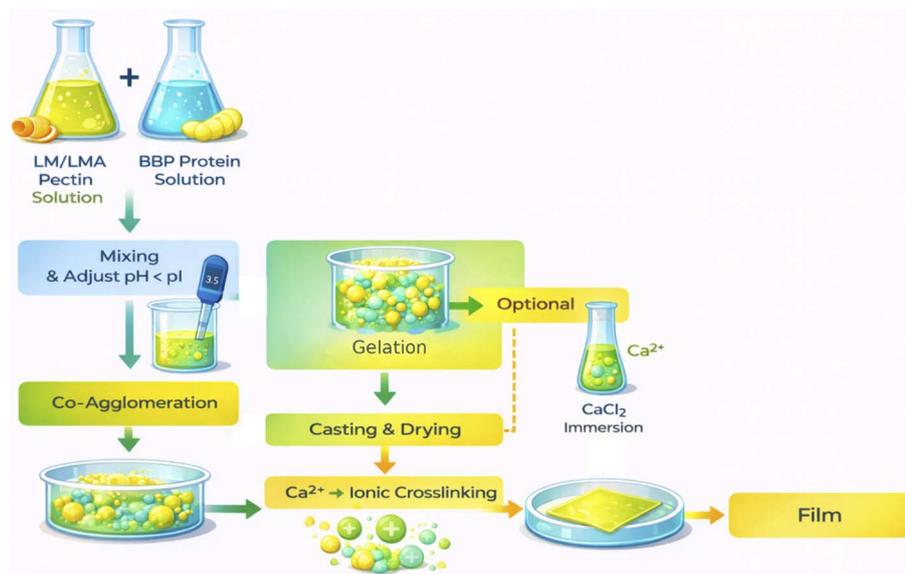

Fig. 1 Co-agglomeration and gelation process.

using a mild alkali treatment in an ethanol–water system (∼70% v/v) at room temperature (0.10 M NaOH, 60 min) to reduce the degree of esterification while limiting backbone cleavage. The reaction was stopped by rapid heating, followed by ethanol precipitation and drying to obtain LM-pectin.

(4) Amidation to obtain LMA-pectin: the LM-pectin was amidated in a cold ethanol–water suspension (∼70% v/v) using ammonia (NH_4OH/NH_3) at 5 °C for 60 min. The suspension was then neutralized to approximately pH 6.5, and the product was recovered by ethanol precipitation and drying to yield low-methoxyl amidated pectin (LMA-pectin).[36]

(5) Storage: the final pectin was stored in sealed containers under cool and dry conditions (25 °C, RH < 40%) until use in film fabrication, including blending with bee pupa protein at pH below the protein pI and subsequent $CaCl_2$ reinforcement (immersion) when applicable.

2.2. Bee pupa protein extraction (BBP)

Honey bee pupae (*Apis mellifera*) collected from a honey bee farm (Hai Phong, Vietnam) after being separated from the hive were quickly processed within 24 hours: cold water washing, blotting dry, rapid enzyme inactivation by very short blanching (≈100 °C, 40 s), defatting with food solvent to increase extraction efficiency and improve protein functionality. The solvent used was 95% ethanol at 50 °C, ratio 1 : 10 (w/v), treated twice for 30 min each, gently stirred then centrifuged, and dried to ∼6–8% moisture. The defatted pupae powder was dissolved in mild alkali according to the standard method for insect proteins: dispersed at a solid : liquid ratio of 1 : 10 (w/v) in distilled water, adjusted to pH 10.0 with 0.1 M NaOH, added "salting-in" salt (0.5 M NaCl), stirred at 25 °C for 60 min (ultrasonication at 40 kHz for the first 10 min), and centrifuged to remove the insoluble phase (very low cuticle/chitin fragments in pupae) to obtain the protein extract.[25,37,38] The alkaline extract after filtration was adjusted to pH ∼5.0 near the isoelectric point (pI) for isoelectric precipitation to obtain crude BBP. The precipitate was washed with cold water (two to three times at pH ∼5.0) and then slightly neutralized (pH 6.5–7.0), lyophilized or freeze-dried ≤45 °C to obtain the BBP isolate. Mild enzymatic hydrolysis using Alcalase (pH 8.0, 50 °C, 30 min) was performed to generate functional peptides.[39]

To ensure safety and reproducibility, the entire defatting–alkali extraction–isoelectric precipitation step was operated under hygienic conditions, with the alcohol solvent recycled by distillation and neutralization of acid/alkali wastewater before discharge; the BBP product was packaged in a moisture-proof package and stored at ≤25 °C, RH < 40% until mixing with pectin at pH below pI to form a complex charge during film casting.

2.3. Food film manufacturing

The casting solution was prepared using an aqueous slurry (solvent–slurry) method, in which the components were dispersed in water to promote pectin–protein co-aggregation, followed by post-casting Ca^{2+} ion reinforcement. Orange peel pectin (LMA) was dissolved in distilled water to a concentration

of 2.5% (w/v) at 70 °C under stirring, cooled to 25 °C, and the system pH was adjusted to 4.6–4.9 with citric acid; this pH range was chosen so that the bee pupal protein (BBP) when added would be positively charged compared to the negatively charged pectin, creating a uniform electrolytic complex in the casting solution. After reaching the target pH, BBP was added in portions to reach 0.3–0.5% (w/v) (according to the casting solution), followed by 20–30% glycerol calculated on the total polymer solids to create plasticity; the mixture was defoamed by vacuum for 3–5 min and allowed to rest for 10 min before casting. The choice of pectin concentration, pH window, co-aggregation mechanism and plasticizer ratio was referenced from modern pectin film fabrication reviews/procedures and from studies on pectin–protein (whey) electrolyte complexes as the technological benchmark for pectin–BBP hybrid systems.[1]

The casting solution was spread on a non-stick flat surface (Teflon) using a scraper to achieve a wet thickness of 0.50–1.00 mm (expected dry thickness 50–100 μm depending on the configuration), and forced-dried at 35–40 °C until surface dry. The surface-dried films were then dipped in 1.0–2.0% (w/v) $CaCl_2$ for 1–2 min at 25 °C, then drained and dried to completion at 35–40 °C; the Ca^{2+} dipping step was intended to form an "egg-box" network on the homogalacturonan region of the LM/LMA pectin, thereby increasing tensile strength and reducing moisture penetration, a widely described and used standard procedure for pectin and pectin-blend films. After drying was complete, the film samples were peeled off the substrate and conditioned at 25 °C, 50% RH for at least 48 h.[34,40] A three-factor Central Composite Design (CCD) experiment was designed with randomization of run order and daily blocking to control environmental variation. The three independent variables and the investigated domain were set as follows: BBP ratio (A) 0.10–0.70% (w/v) to cover the region below–above the optimal co-agglomeration threshold; glycerol (B) 20–30% (on dry polymer) for the plasticity–stability balance; $CaCl_2$ immersion concentration (C) 0.5–2.0% (w/v) to cover the ion network formation region without film embrittlement. Pectin (LMA) was fixed at 2.5% (w/v), mixing pH was fixed at 4.7, immersion temperature was 25 °C, and immersion time was 90 ± 30 s.

2.4. Physicochemical properties of food films

The thickness of the film samples was measured using a digital micrometer (Mitutoyo, 293-240-30, Japan), at ≥10 points/slab and averaged; following ASTM D6988 (Guide for Determination of Thickness of Plastic Films When Thickness Is Used Directly in Calculating Properties), with attention to flat surfaces and repeatable pressure between measurement points. Tensile mechanical properties were determined on a Universal testing machine (Galdabini, Quasar 50 kN, Italy) according to ASTM D882 on strip specimens (100 × 10 mm specimen size, 50 mm clamping distance, 50 mm min^{-1} tensile speed), calculating tensile strength (TS), elongation at break (EAB) from maximum load–elongation and cross-sectional area calculated by thickness average, and storage elastic tissue E' (DMA E') according to ASTM D4065. Water vapor permeability (WVP) was measured by the weighed cup method (ASTM E96/E96M,

desiccant or water method depending on the configuration), with the cup containing anhydrous CaCl$_2$ (desiccant) placed in an air atmosphere of 75% RH (saturated NaCl) at 23 °C or the specified test conditions; the mass increase over time was monitored to derive the water vapor transmission rate (WVTR) (g per m^2 per day), then WVP = (slope × L)/(A × Δp) was calculated, where the slope is the steady-state mass increase rate, L the average thickness, A the exposed area, and Δp the water vapor pressure difference on either side of the sample.

The moisture content of the sample was determined by the AOAC air-oven (Binder, FD 115, Germany) method (AOAC Official Method 925.10), by drying at 105 °C in a ventilated convection oven until constant mass was achieved; water solubility was determined by soaking in distilled water for 24 hours at 25 °C, filtering, drying the residue to constant mass and calculating the percentage of soluble solids according to the Gontard method commonly used for edible films; this is the common reference procedure in publications on polysaccharide/protein films.[41]

Oxygen permeability (OTR) and specific oxygen permeability (permeability) were determined according to ASTM D3985 using a coulometric sensor on an XHinstruments XHS-OTR instrument (XHS-OTR, China), at 23 °C under defined humidity conditions and effective area according to the measuring chamber; OTR (cm^3 per m^2 per day) is corrected for thickness to derive OP (cm^3 m per m^2 per day per kPa) for homogeneous materials.

Optical properties were assessed by ultraviolet-visible (UV-Vis) spectroscopy (200–800 nm) on a UV-Vis spectrophotometer (Hitachi, U-2900, Japan): T_{280} (UV blocking ability) and T_{600} (visible transparency) were used as quick indices; haze (BYK-Gardner, haze-gard i, Germany) and light transmittance were measured according to ASTM D1003 to provide comparison parameters between formulations. CIE Lab* color coordinates were calculated from the transmission/reflectance spectra according to ASTM E1164 (requires measurement, calibration, and geometry) and ASTM E308 (D65 illumination, 10° standard observer (CIE 1964)).

Attenuated total reflectance-Fourier transform infrared spectroscopy (ATR-FTIR) spectra were recorded in the 4000–400 cm^{-1} range on a ATR-FTIR spectrometer (Agilent, Cary 630, USA) to monitor the ester/acid carbonyl groups of pectin and the amide I/II bands of proteins. TGA/DSC thermal analysis was performed on a thermogravimetric analyzer (LINSEIS, TGA PT 1600, Germany) with heating rate 10 °C min under a nitrogen (N$_2$) atmosphere and sample mass 5 mg.

Scanning electron microscopy (SEM) was employed to examine the film cross-sections using a JSM-IT200 instrument (JEOL, Japan) operated at room temperature (≈25 °C). Prior to imaging, the specimens were cryofractured by immersion in liquid nitrogen and fractured to obtain a clean cross-section, dried, and sputter-coated with a thin platinum layer. Micrographs were acquired at an acceleration voltage of 10 kV and used to evaluate the film microstructure and phase uniformity.

The Z-average particle size was determined by laser scattering on an LA 960 system (HORIBA, Japan). The LMA–BBP pectin co-agglomerate was prepared in ultrapure water (18.2 MΩ cm), keeping the polymer ratio as in the casting solution, reducing the total solids by ∼0.10% w/v, adjusting the pH with 0.1 M HCl/NaOH, shaking for 10 s and leaving it for 5 min at 25 °C before measurement.

The charge properties of LM/LMA pectin, BBP, and their mixtures were evaluated by zeta potential (ζ) measurements using a zeta potential analyzer (Malvern Panalytical Zetasizer Nano ZS, UK) based on electrophoretic light scattering. Samples were diluted to 0.10 mg mL^{-1}, adjusted to the target pH using 0.1 M HCl or 0.1 M NaOH, equilibrated for 10 min, and measured at 25 °C in disposable folded capillary cells.

All measurements were performed according to the pre-test conditioning according to ISO 291 and were performed on at least three independent film plates ($n = 3$), each plate taking at least three replicates for the same index; the data are averaged ± standard deviation, used for statistical processing and formula optimization in the following sections.

2.5. Safety assessment and application in food preservation

This section describes the experimental procedures to (i) validate the safety of orange peel pectin (LM/LMA)–bee pupal protein (BBP) films by heavy metal, microbiological and biodegradation tests, and (ii) implement the preservation of real samples of tomatoes and beef using the optimal coatings established in the previous sections. All tests were performed according to the principles of laboratory quality control (blank, certified reference/CRM, matrix recovery, at least $n = 3$ replicates) and record environmental conditions (temperature/humidity/CO$_2$) during storage. For heavy metal analysis, film samples (cut into ∼5 × 5 mm) were microwave digested in PTFE vessels with HNO$_3$ (65%, w/w) and H$_2$O$_2$ (30%, w/w), and measurements were performed by ICP-OES: recovery 80–120% on CRM/matrix standard, relative standard deviation (RSD) ≤10%, and limit of detection (LOD/LOQ) 0.03 ppm.

Microbiological analysis was carried out in parallel on films and on food samples according to peer ISO standards for the food chain: total aerobic count at 30 °C by the pour plate/surface plating technique according to ISO 4833-1; Enterobacteriaceae according to ISO 21528-2; E. coli β-glucuronidase positive on TBX at 44 °C according to ISO 16649-2; Staphylococcus aureus (coagulase positive staphylococcus) on Baird-Parker according to ISO 6888-1; Salmonella spp. (presence/25 g) according to ISO 6579-1; Listeria monocytogenes detected according to ISO 11290-1 and quantified according to ISO 11290-2 when required. Results reported as CFU g^{-1} (log$_{10}$) or presence/25 g for detection; incubation conditions and culture media comply with each standard.

Biodegradation of the film was assessed by the percentage loss of mass after a defined incubation period. Samples were cut into 20 × 20 mm pieces, recorded on initial dry mass, placed in mesh bags, and monitored periodically (every 7 days).

The storage procedures for real samples – tomatoes (12 °C) and beef (4 °C) were designed to be consistent to evaluate the coating performance. Tomatoes were obtained from Hoang Nam Phat Cooperative, Haiduong, Vietnam. Uniformly ripe red tomatoes (no bruises, no diseases) were washed under clean

water and lightly sterilized with 100–150 ppm sodium hypo-chlorite (NaOCl) for 2 minutes and air-dried. Beef samples were obtained from Vifood Company, Haiduong, Vietnam. The beef was collected fresh, immediately after slaughter, and was not processed. Beef (sirloin) was sliced 10 × 10 cm, ~1 cm thick, free fat removed, handled under cold conditions (≤10 °C). Optimum coating: 2.5% w/v LMA pectin + 0.5% w/v BBP, 25% glycerol (based on polymer solids), was wrapped around the study samples. Recommended sample size: 10 tomatoes/lot × 3 replicates ($n = 30$) and beef 6 trays/lot × 3 replicates (2 slices per tray). Comparison group: (i) control without coating, (ii) pectin-single coating, (iii) pectin–BBP coating. Packaging and storage: tomatoes in PET trays with perforated lids for gas exchange (≈ 10 holes/Ø 1 mm), stored at 12 ± 0.5 °C; 85–90% RH; beef in PS trays, covered with air-permeable PVC overwrap, stored at 4 ± 1 °C. Sampling schedule: tomatoes days 0–4–8–12; beef days 0–3–6–9–12. At each time point, record weight loss (before/after weight, %), firmness, pH, and microbiology; for beef, a lipid oxidation index (TBARS) may be added. All microbiological measurements comply with the relevant ISO; sample handling and recording follow the laboratory biosafety guidelines (BSL-2) and ISO 6579-1/11290-1 for safe handling.

3 Results and discussion

3.1. Effect of the BBP ratio

When increasing the BBP content from 0 → 0.5% w/v, TS increased almost linearly and then reached a maximum around 0.5% (Fig. 2a), while EAB also reached a maximum at the same concentration (Fig. 2b). At the same time, WVP and OTR decreased sharply and appeared at the same optimum point at 0.5% (Fig. 2c and d). After this threshold (0.7%), TS/EAB decreased slightly, while WVP/OTR increased again; at the same time, T_{600} decreased and haze increased almost linearly with BBP (Fig. 2e and f). This synchronous maximum–minimum pattern is typical of electrolytic coacervation between positive protein and negative pectin at approximately neutral charge ratios: in the region near charge equilibrium, the density of electrostatic–hydrogen bonds reached a maximum, the coacervation network was compressed, thus increasing both strength–flexibility and reducing the free volume for water vapor/oxygen diffusion; beyond this ratio, excess protein leads to protein-rich/mismatched microphase domains, causing microscopic defects and light scattering (opacity) with increased ventilation/humidity.[42]
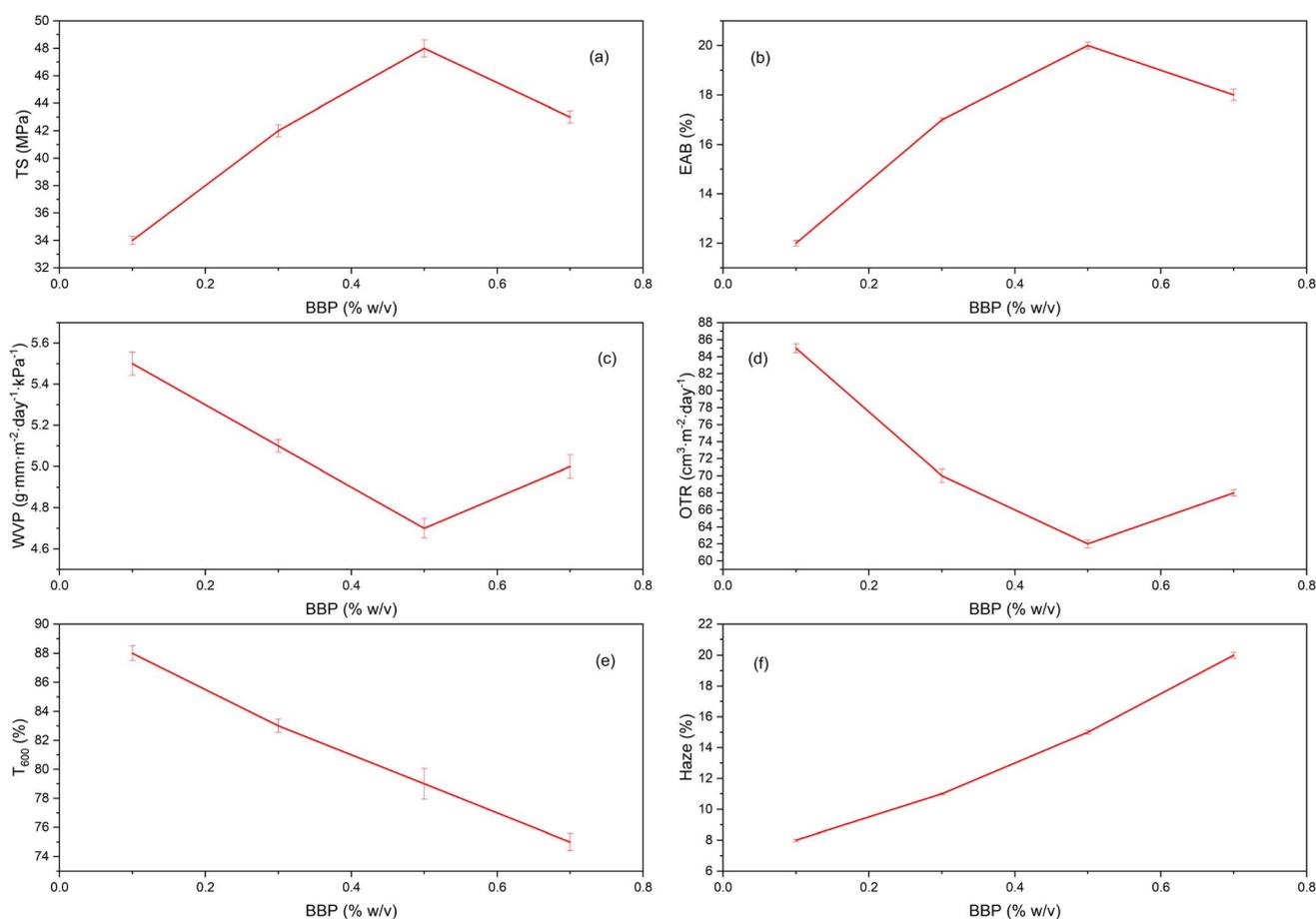

Fig. 2 Effect of bee pupal protein (BBP) content on film properties: TS (tensile strength) (a); EAB (elongation at break) (b); water vapor permeability (WVP) (c); oxygen permeability (OTR) (d); T_{600} (transparency in visible range) (e) and haze (f). Manufacturing conditions: pectin (LMA) 2.5% (w/v), glycerol 25% (w/v), CaCl$_2$ concentration 1.5% (w/v), pH 4.7, temperature 25 °C.

In this study, the Ca^{2+} level was kept constant across all BBP ratios, so the main differences arise from the extent of protein pectin association and the efficiency with which Ca^{2+} reinforces homogalacturonan segments through egg box junction zones. At 0.5 percent BBP, the pectin protein network is sufficiently organized that calcium bridging produces a compact and uniform dual network consisting of an electrostatic complex and a Ca^{2+} mediated pectin framework. This structure supports high tensile strength, while elongation at break remains acceptable due to plasticization by glycerol. At the same time, water vapor and oxygen transport decrease because a denser microstructure and reduced free volume increase the tortuosity of diffusion pathways. The structural basis of calcium junction formation in LM and LMA pectin networks and the associated reduction in molecular mobility have been widely described for pectin and alginate systems, and these concepts can be extended to protein pectin hybrid films. A slight decline in tensile strength and elongation at break at 0.7 percent BBP, together with higher WVP and OTR, can be attributed to two effects. First, when protein exceeds the effective binding capacity of pectin, protein rich aggregates and discontinuous microdomains may form, reducing homogeneity and creating preferential pathways for gas and water transport. Second, a higher protein fraction can increase bound water and overall moisture affinity, which tends to raise WVP, a trend commonly reported in protein based films once the optimal blending threshold is exceeded. In optical terms, the decrease in transmittance at 600 nm and the increase in haze with increasing BBP are consistent with stronger light scattering caused by refractive index contrast and microstructural heterogeneity, which can be described by Mie type scattering (light scattering by particles/aggregates with sizes comparable to visible wavelengths) and has been observed in other films containing protein additives or protein polysaccharide complexes.[43]

Regarding barrier function, the lowest OTR at 0.5% BBP is in line with the general trend: the interaction-rich network of biofilms can limit oxygen diffusion better than a single polysaccharide matrix, especially when ionic bonds and equilibrium moisture levels are present; classic studies on edible films have also reported an optimum protein/polysaccharide system for gas barrier compared to each individual phase. Combined with a minimum WVP of 0.5%, this can be considered the optimum BBP ratio for the mechanical–barrier–optical balance: TS/EAB do not cancel each other out, the moisture–gas barrier is improved, and the clarity remains acceptable for fresh coatings.

More broadly, a bell-shaped response to protein content has been observed in many protein–polysaccharide systems: with excess protein, films are generally more opaque, locally brittle, and more permeable to moisture; with protein deficiency, the bridges are insufficient to reinforce the pectin network. Recent reviews have again emphasized the role of charge design (pH vs. pI, methoxyl/acetyl degree of pectin) and the ion valence level in achieving the optimum structure–function of hybrid complexes/films. Thus, the results are consistent with the international theoretical and experimental basis for protein–pectin co-aggregation and Ca^{2+} reinforcement.[44]

In summary, 0.5% w/v BBP is the most effective region for the LMA–BBP–Ca^{2+} pectin system: maximizing effective strength and flexibility, minimizing WVP/OTR, at the expense of a moderate reduction in clarity; when BBP was increased to 0.7%, the structure began to oversaturate, leading to mechanical and barrier deterioration and opacity. This conclusion is based on the characteristic manifestations of near-neutral coacervation and "egg-box" crosslinks in pectin, as well as on the understanding of the microstructure–moisture/gas-optical relationship of biofilms.

3.2. The role of pH and coacervation

The pH influence data range (Fig. 3) and pH–salt correlation (Fig. 4) show a very narrow coacervation window around pH $\approx$ 4.6–4.8: at which the OD_{600} turbidity reaches a maximum (heat map), the DLS particle size increases sharply, and zeta approaches 0 mV; at the same time, the TS/EAB of the film peaks and the WVP, T_{600} bottom out, and haze increases sharply. This is a typical signature of electrolytic coacervation between positively charged protein (near pI) and negatively charged pectin (above $pK_a \approx 3.5$, so negatively charged in the investigated pH range): when the net charge of the protein–polysaccharide phase approaches neutralization, the system forms a dense complex rich in electrostatic–hydrogen bonds, causing increased scattering (turbidity) in the solution, increasing the size of the aggregate, and when casting the film, it will give a densely packed polymer network that is more durable and less permeable. The maximum turbidity near $\zeta \approx 0$ mechanism and the pH–zeta–aggregation relationship have been established in whey/pectin, gelatin/pectin, gum arabic/milk protein systems and many other protein–polysaccharide pairs. The effect of ionic strength also has an optimal shape: OD_{600} is the largest at 10–15 mM NaCl, decreasing gradually when [NaCl] $\geq$30–40 mM. At low–moderate salts, ions shield the repulsive forces between like-charged patches on the complex surface, helping them to come close and aggregate effectively, while high salts shield the electrostatic attraction, causing the complex to disintegrate/no longer coacervate. This observation is consistent with experiment and modeling in many protein–polysaccharide systems, where the OD curve or phase diagram shows an optimal salt window and inhibition of coacervation at high ionic strength.[45,46]

Charge-wise, when increasing pH from 4.0 → 6.0, the zeta of the mixture shifts from negative to slightly positive, cutting off 0 mV near 4.6–4.8, the point where the OD_{600} and DLS size co-maximum (coincident maxima of turbidity (OD_{600}) and DLS aggregate size near zeta potential ∼0 mV, indicating strongest complexation/coacervation). This suggests that the charge ratio between BBP and pectin in this region approaches neutrality, forming a polymer-rich coacervate. Several studies using turbidity–DLS–ζ also reported a turbidity/size peak at $\zeta \approx 0$ and in the pH range characteristic of the interaction pair.[47,48]

The effect on film properties directly reflects the coacervate microstructure. At the optimal pH, TS and EAB increase simultaneously (the interconnected network is dense but still lubricated by glycerol), while WVP and T_{600} decrease due to the
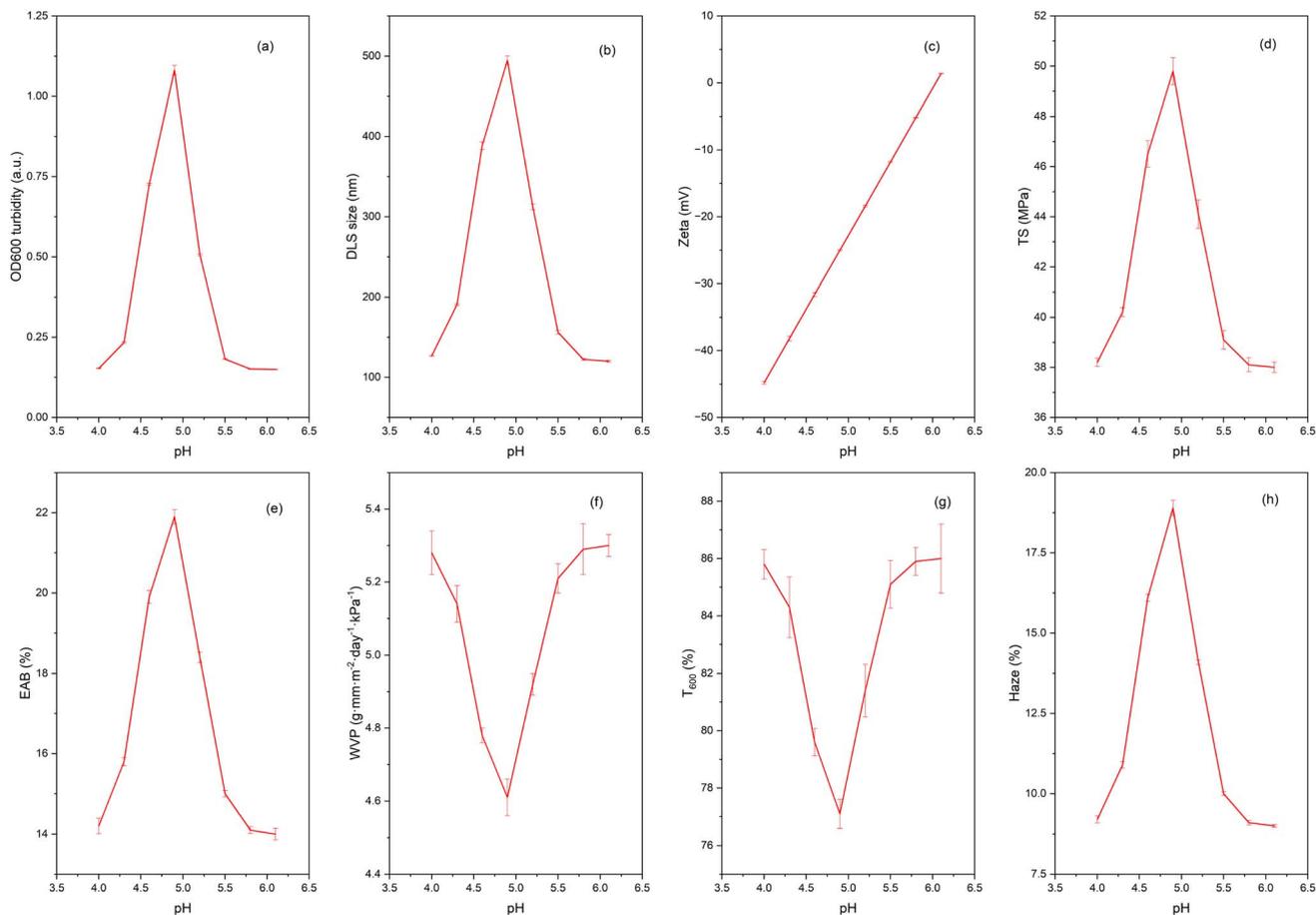
Fig. 3 Effect of pH on film properties: OD600 turbidity (a); DLS size (b); zeta (mV) (c); TS (tensile strength) (d); EAB (elongation at break) (e); water vapor permeability (WVP) (f); T_{600} (transparency in visible range) (g) and haze (h). Manufacturing conditions: pectin (LMA) 2.5% (w/v), glycerol 25% (w/v), $CaCl_2$ concentration 1.5% (w/v), BBP 0.5% (w/v), temperature 25 °C.

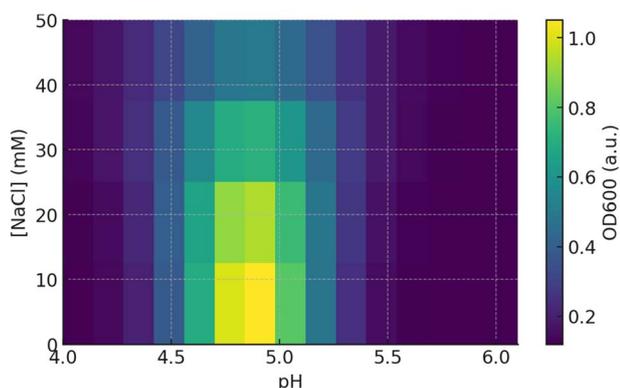**Fig. 4** OD_{600} correlation map according to pH and ionic strength (NaCl) of the LMA–BBP system.

reduced free volume and diffusion path; when moving out of the pH window (4.3 or 5.6–6.0), the coacervate dilute is unstable, leading to a less homogeneous film, an increase in T_{600} again, and a decrease in haze. Recent reviews and whey/pectin systems have noted that a narrow pH window governs the coacervate thickness–thinning, and thickness is related to the barrier strength of the film after casting.

The role of pectin structure is also important. LM/LMA pectin has a high carboxylate density (negatively charged above pH > ~3.5), which favors electrolytic interactions with proteins; at the same time, the amidation nature modifies the charge–hydration distribution, softens the isoelectric transition, and creates a more suitable pH window for uniform aggregation. Studies on LM/LMA pectin in milk/protein systems also show that adjusting the pH–ion–mixing ratio will strongly change the microstructure and mechanics of the gel/complex.[49]

In summary, our data fit a pH- and ionic strength-driven coacervation model: pH ~4.6–4.8 ($\zeta \approx 0$) and low–moderate NaCl (≈ 10–15 mM) produce the densest and most stable coacervates, transforming into films with high TS/EAB and low moisture–gas barriers; outside this window, aggregation weakens, the film network becomes more fluid–deficient, and performance deteriorates. This principle is consistent with known protein–polysaccharide systems and with the electrophilic behavior of LM/LMA pectin in food environments.

3.3. Effect of Ca^{2+} and the egg-box mechanism

The $CaCl_2$ concentration range shows a clear optimum around 1.5% w/v: TS and EAB increase and then decrease slightly above

the threshold; WVP and OTR decrease to a minimum at ~1.5% and then increase again; DMA E' and FTIR cross-linking index also peak near this region (Fig. 5). Such a synchronous peak-trough response pattern is typical of the LM/LMA pectin network that is densified by Ca^{2+} *via* an egg-box mechanism on the homogalacturonan segment (Fig. 6): Ca^{2+} ionically bridges the two –COO^- chains, creating densely interconnected regions (junction zones) that increase network density, reduce free volume and lengthen the diffusion path of moisture/gas; thus, mechanical strength (TS, E') increases and WVP/OTR decreases as Ca^{2+} increases from low to medium levels. The egg-box mechanism and selectivity of Ca^{2+} to polyuronates have been modeled and experimentally demonstrated for pectin LM (similar to alginate), where medium doses of Ca^{2+} create the tightest network, while too high doses weaken the beneficial interaction.[50] When $CaCl_2$ is increased beyond ~2.0–2.5%, the decrease in TS/EAB and the slight increase in WVP/OTR can be attributed to network over-determining and charge shielding: the too high density of Ca^{2+} spheres makes the network brittle and less flexible, easily causing micro-defects/micro-cracks during the drying-conditioning process, and at the same time, excess Ca^{2+} shields the electrostatic attraction between negative pectin and positive protein domains, reducing microstructural

uniformity; both factors cause the moisture/gas barrier to deteriorate even though the total number of ionic bonds increases. The tendency for barrier–mechanical improvement at moderate Ca^{2+} doses and deterioration at overdose has been widely documented in pectin films/gels and related polysaccharides.[51]

The increase of E' (DMA) with $CaCl_2$ up to the optimum region reinforces the thicker network → higher stored elasticity argument: as the number of "egg-boxes" increases, elastic deformation is better stored at low frequencies, so E' increases; above the threshold, salt heterogeneity and micro-brittleness cause no further increase or decrease of E'. The tendency of E' to increase with the level of Ca^{2+} cross-linking has been reported for pectin and pectin-hybrid systems (measured in film tension/DMTA mode).[52,53]

Regarding the spectroscopic evidence, the increased FTIR cross-linking index in the Ca^{2+} optimum region is consistent with the intensity shifts/variations of the symmetric (~1400–1440 cm^{-1}) and asymmetric (~1585–1600 cm^{-1}) COO^- bands, sometimes accompanied by changes in the OH region due to ion–hydrogen bridge formation; FTIR reviews/data on pectinate Ca^{2+} and OM–cation both describe these shifts as traces of Ca^{2+} coordination.[30]
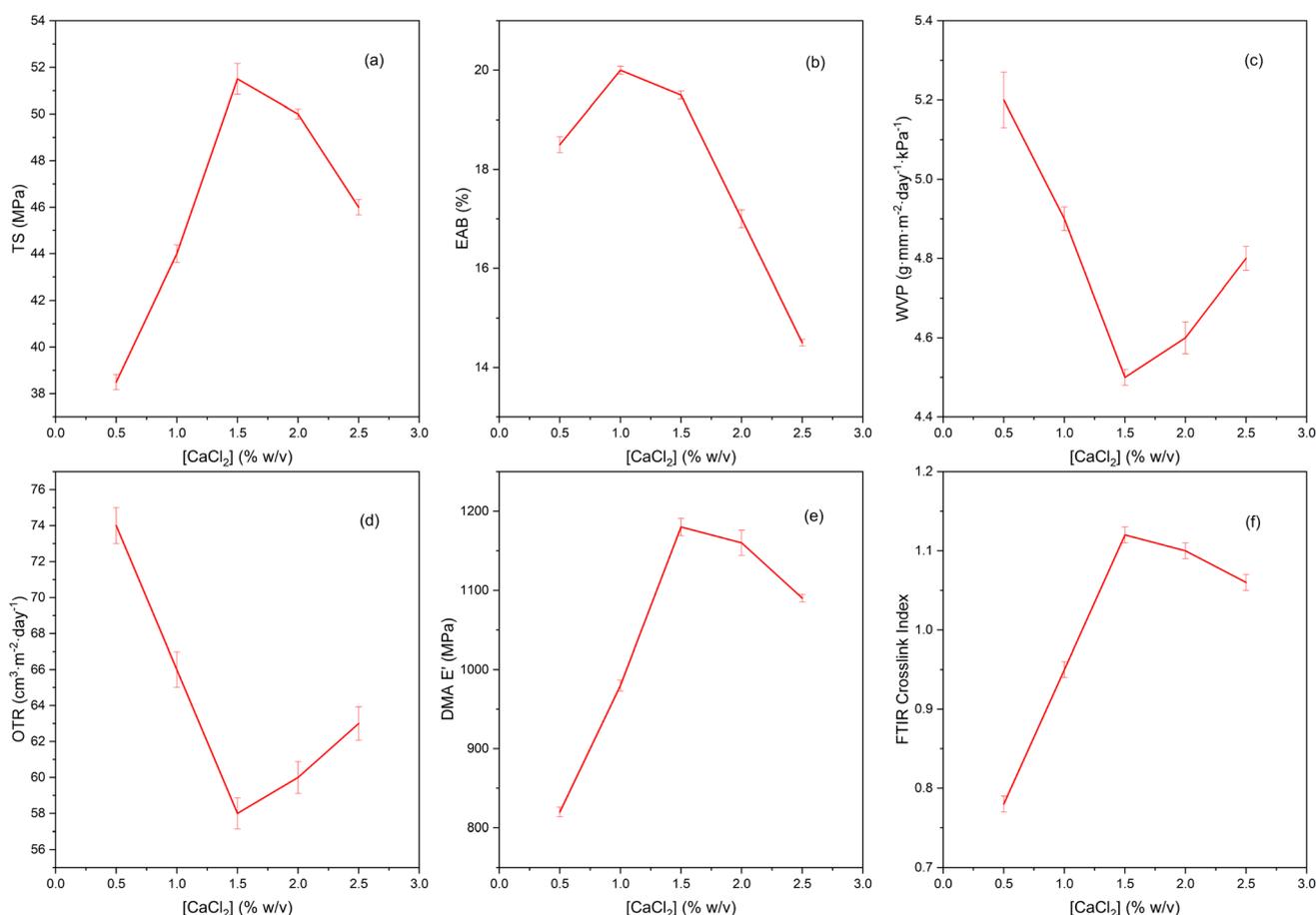

Fig. 5 Effect of $CaCl_2$ concentration on film properties: TS (tensile strength) (a); EAB (elongation at break) (b); water vapor permeability (WVP) (c); oxygen permeability (OTR) (d); storage modulus (E') in DMA (e) and FTIR crosslink index (f). Manufacturing conditions: pectin (LMA) 2.5% (w/v), glycerol 25% (w/v), BBP 0.5% (w/v), pH 4.7, temperature 25 °C.

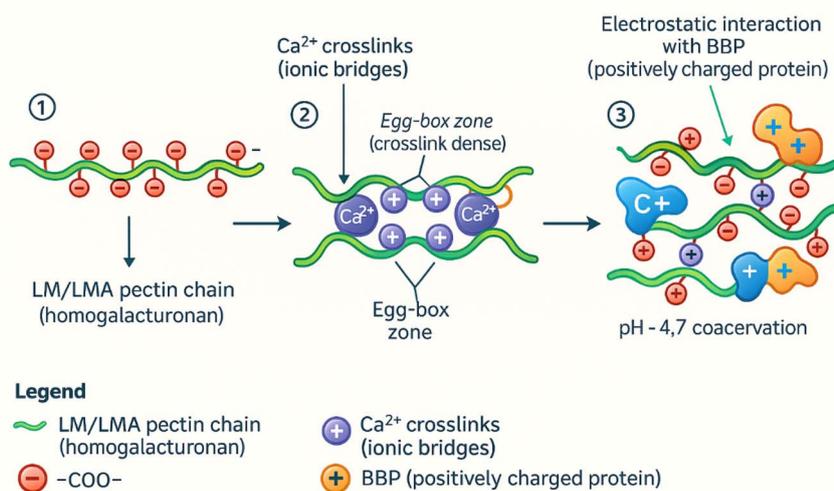**Fig. 6** "Egg-box" mechanism in the LMA–BBP film.

The moisture barrier effect of Ca^{2+} is generally improved at moderate doses due to less hydration of the network and tortuous diffusion paths; several studies with $CaCl_2$ treated pectin/alginate films show a clear decrease in WVP with increasing Ca^{2+} from low to medium, consistent with our WVP minimum at ∼1.5%.

The combined TS/EAB, WVP/OTR, E' (DMA) and FTIR observations suggest that Ca^{2+} acts as a structural reinforcement *via* an egg-box mechanism with an optimum window around 1.5% w/v $CaCl_2$: below this level the bond is not sufficiently thick and the mechanism-barrier is limited; above this level, the network becomes too stiff and heterogeneous, leading to brittleness and micro-defects, which reduce strength and increase permeability. This observation is consistent with the classical egg-box model and recent reviews of pectin–Ca^{2+} gels/films.

3.4. Glycerol effects

When the glycerol content (calculated on the total polymer basis) was increased from 15 to 35%, the LM/LMA–BBP pectin films progressively transitioned from a tightly hydrogen-bonded glassy regime (restricted segmental mobility) to a more flexible state with higher chain mobility and effective free volume. This transition was consistently reflected across all measured properties: TS decreased nearly linearly, whereas EAB increased steadily; T_g dropped markedly and the equilibrium moisture content increased, confirming the plasticization effect of glycerol. In parallel, the barrier performance changed in the same direction, with WVP and OTR increasing simultaneously, indicating facilitated mass transport through the more mobile matrix. The water contact angle also decreased, suggesting a more hydrophilic surface associated with higher glycerol/moisture affinity (Fig. 7). The dominant mechanism is the classical plasticizing effect: small glycerol molecules, poly –OH insert into the pectin–protein hydrogen bond network, reduce the density of secondary bonds, increase the free volume and increase the chain mobility, so the material is softer and more flexible (EAB↑, T_g↓) but has lower tensile strength and lower barrier (TS↓, WVP/OTR↑). This trend is typical of polysaccharide/protein films and has been extensively reviewed in reviews of plasticizers for biofilms.[54]

In pectin films, several experimental studies have shown that with increasing glycerol, TS decreases, EAB increases, and WVP increases due to water and glycerol acting together as hydrophilic plasticizers; the authors also noted a higher moisture sensitivity of plasticized pectin films. Our observations (TS↓, EAB↑, WVP↑) are consistent with the results on pectin films and are also consistent with starch/protein: adding glycerol increases water vapor permeability and decreases stability, because the diffusion path for small molecules (H_2O/O_2) becomes shorter and less tortuous as the free volume increases.[55] The increase in OTR with glycerol can be explained by increased glycerol mobility and decreased packing, similar to what was observed in whey protein systems: when glycerol was reduced or partially replaced by a more structural/protein phase, OTR/WVTR decreased, implying that glycerol is the agent that causes a poorer gas barrier beyond its optimum.[56] The balanced increase in wettability and decrease in contact angle with increasing glycerol reflect the hygroscopic and hydrophilic nature of glycerol: the –OH groups orient the surface, pulling down the surface tension, improving water wetting and increasing the network's hygroscopicity; a similar phenomenon has been described for pectin and gelatin with increasing glycerol, where the contact angle decreases significantly and the wettability/solubility increases.[57]

Optically, T_{600} peaks at medium glycerol levels and then decreases at higher levels, while haze has a U-shape: medium
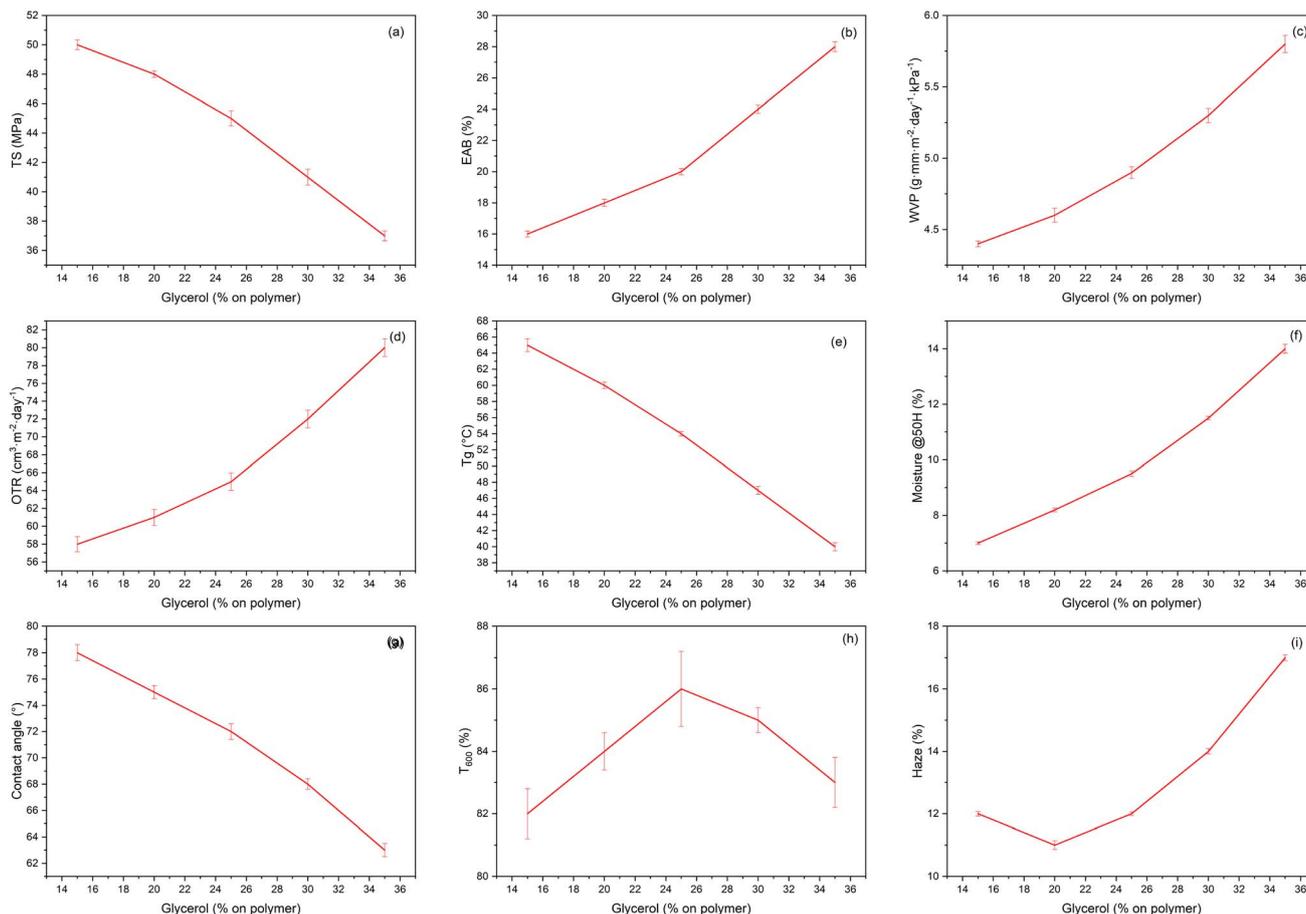
Fig. 7 Effect of glycerol on film properties: TS (tensile strength) (a); EAB (elongation at break) (b); water vapor permeability (WVP) (c); oxygen permeability (OTR) (d); glass transition temperature (T_g) (e); moisture @ 50% RH (f); contact angle (g); T_{600} (transparency in visible range) (h) and haze (i). Manufacturing conditions: pectin (LMA) 2.5% (w/v), glycerol 25% (w/v), BBP 0.5% (w/v), pH 4.7, temperature 25 °C.

doses help reduce internal stress – fill microcracks, resulting in better light transmission; but at high doses, adsorbed water and microheterogeneities due to excess glycerol/high humidity create stronger scattering → increased opacity. Pectin–glycerol optimizations have documented a glycerol window for the most balanced clarity and mechanical properties, reinforcing this interpretation.[16]

Taken together, the data suggest that glycerol is the variable controlling the optical-barrier–plasticity of pectin–BBP films: increasing glycerol increases plasticity but at the expense of moisture/gas barrier and surface hydrophobicity. Therefore, choosing a medium level (*e.g.*, around 25–30% on polymer solids) often achieves the best mechanical–barrier–optical balance for preservative coating applications, while too high a dose makes the film less barrier, more hydrophilic, and more opaque, in line with current understanding of plasticization in edible films.

3.5. Evaluation of film characteristics

The combined structure–property measurements show that the forms a stable ionic–electrolyte hybrid network, thanks to the egg-box mechanism of Ca^{2+} intercalating the homogalacturonan segment while simultaneously interacting electrostatically with the positively charged domains of the protein, thereby achieving a more balanced optical–barrier–mechanical configuration compared to the two monocomponent films. The combined optical–mechanical data (Fig. 8a) emphasize the synergistic effect of the hybrid network: compared to LMA-only, the LMA–BBP film increases TS (from ~44 → 51 MPa) and reduces OTR (from ~85 → 60 cm^3 per m^2 per day), while keeping EAB at a higher level; compared to BBP-only, the hybrid film improves TS/E' and transparency while retaining good flexibility. The trade-off trend of TS↓/EAB↑/WVP↑ with increasing glycerol and the gas barrier improvement effect of the pectin matrix at medium humidity are both behaviors that have been reviewed for plasticized polysaccharide/protein films.[1,54,58]

The overlapping FTIR spectra (Fig. 8b) clearly demonstrate the characteristics of pectin LM/LMA (ν(C=O) ester ~1730–1740 cm^{-1}; $\nu_{as/s}$(COO$^-$) ~1600/1440 cm^{-1}; 1240–1145–1050 cm^{-1} region of C–O/C–O–C), which are widely used to infer the amidation/esterification degree and cation coordination of pectin; in the hybrid film, the protein amide I/II bands (~1650/1545 cm^{-1}) and the slight shift of the COO$^-$ band ($\approx$1605 cm^{-1}) are consistent signatures of Ca^{2+} coordination and pectin–protein interactions in the network. This interpretation closely
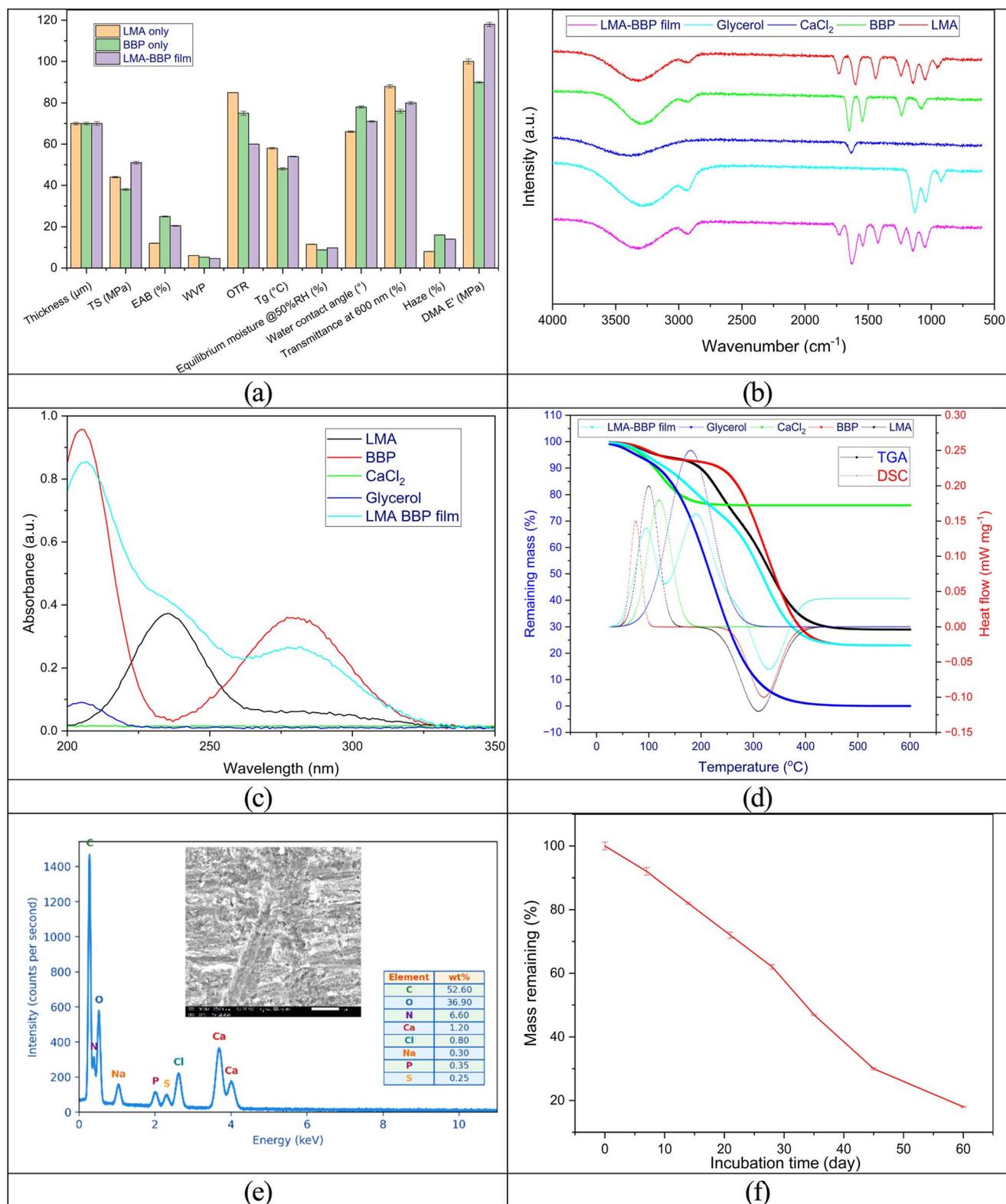
Fig. 8 Characterization of the films. (a) Summary of key physical/mechanical, barrier, optical and thermal properties for LMA-only, BBP-only and LMA−BBP hybrid film. (b) ATR−FTIR spectra of LMA, BBP, CaCl₂, glycerol and the LMA−BBP film. (c) UV-vis spectra of the same components. (d) TGA/DSC thermograms. (e) SEM micrograph and EDS elemental analysis of the LMA−BBP film. (f) Biodegradation profile under laboratory composting.

follows experimental/quantitative DM FTIR for pectin (correlation $1740/(1740 + 1600$ cm^{-1})) and recent reviews of the pectin–Ca^{2+} structure.[59]

The UV-Vis results (Fig. 8c) are consistent with the chemical composition: the BBP sample exhibits strong peaks at ~205 nm (peptide backbone) and ~280 nm (Tyr/Trp aromatic chain), the LMA has only a weak shoulder at ~235 nm, the glycerol/CaCl$_2$ is almost transparent; the spectrum of the LMA–BBP film is a combination of the above traces plus a slight scattering background of the film. TGA/DSC (Fig. 8d) reinforces the structural picture: both pectin and hybrid films exhibit a moisture loss step of ~90–120 °C, followed by glycerol loss/evaporation of ~170–220 °C (when present), and polysaccharide backbone decomposition of ~230–350 °C; the residual mass (char/ash) at 500–600 °C represents the nonvolatile fraction remaining after thermal decomposition, arising from carbonaceous char formation and any inorganic mineral residue (salts/ions) present in the films. The DSC T_g of ~54 °C of the film matches the observed effective viscosity (EAB ~20.5%). This multistep pectin curve and characteristic decomposition temperature are consistent with recent TGA reports of pectin/pectin films in the literature.[60,61]

The SEM-EDS result (Fig. 8e) shows that the hybrid film surface and cross-section are relatively smooth, denser than the monocomponent film, with fewer micro-pores, characteristics typically associated with longer moisture/gas diffusion paths and higher tensile strength in ion-reinforced polysaccharide films; this is consistent with the measured physical properties. The EDS results confirm that the LMA–BBP film is dominated by carbon and oxygen (52.6 and 36.9 wt%, respectively), consistent with an organic pectin–protein matrix rich in polysaccharide/protein functional groups. The presence of nitrogen (6.6 wt%) reflects the incorporation of BBP protein into the film network. Importantly, calcium is clearly detected (1.20 wt%) together with a minor chloride signal (0.80 wt%), supporting successful Ca^{2+} uptake from the CaCl$_2$ reinforcement step and suggesting ionic coordination with pectin carboxylate groups that contributes to a more compact and stabilized microstructure, in agreement with the dense cross-sectional morphology observed in the SEM image.

Regarding safety (Table 1), the film's trace levels of Pb/Cd/As/Hg (10^{-3}–10^{-2} mg kg^{-1}) are significantly lower than commonly reported thresholds of concern; EFSA has re-evaluated pectin E 440 (including amidated LMA) and concluded that there is no safety concern for use as a food additive for the general population, no ADI data are required. The background microbiological profile is very clean: TPC, yeast–mold <10 CFU g^{-1}, *E. coli*/*Salmonella*/*S. aureus* was not detected, in accordance with the spirit of EC 2073/2005 on microbiological criteria for foodstuffs. The trace metal and microbiological results in Table 1 support baseline safety feasibility for the materials studied. For translation to commercial edible coatings or packaging, compliance should be considered under the applicable frameworks for both food contact materials and edible ingredients. In the European Union, materials intended to come into contact with food are subject to the general safety and traceability requirements of Regulation (EC) No. 1935/2004 and the good manufacturing practice requirements of Commission Regulation (EC) No. 2023/2006. Pectin and amidated pectin have established specifications and conditions of use as permitted food additives (E 440(i) and E 440(ii)) under Regulation (EC) No. 1333/2008 and Commission Regulation (EU) No. 231/2012, and they are also evaluated under Codex and JECFA frameworks. In contrast, insect derived proteins are commonly regulated as novel foods, for example under Regulation (EU) 2015/2283 and the Union list in Commission Implementing Regulation (EU) 2017/2470, with authorisation texts for edible insects noting the possibility of allergic reactions and potential cross reactivity with crustacean and dust mite allergies. Accordingly, further work toward application should include allergen management, controlled sourcing and hygienic processing, and clear consumer information consistent with food information and allergen labelling requirements such as Regulation (EU) No. 1169/2011, together with targeted allergen assays after processing and film formation and exposure or migration assessment under representative use conditions.

The sustainability aspect was confirmed by degradation under laboratory composting conditions: the residual mass decreased rapidly from 100% to ~18% after 60 days, consistent with the high disintegration rates of pectin films previously reported (>50% loss of structure after 2 weeks; ~90% after 3 weeks under some conditions), and in accordance with the ISO 14855 test framework used to assess ultimate aerobic biodegradability and the degree of disintegration under controlled composting. These frameworks/interpretations are now widely used for bio-based packaging materials.[62] From the above pieces, it can be concluded that the LMA–BBP film has a balanced performance profile: toughness–flexibility at the operational level (TS ≈ 51 MPa; DMA E' ≈ 1.18 GPa; EAB ≈ 20.5%), good gas barrier for a hydrophilic film (OTR ≈ 60 cm^3 per m^2 per day), moderate moisture barrier (WVP ≈ 4.6 g mm per m^2 per day per kPa) but can be fine-tuned with glycerol/humidity, adequate clarity (T_{600} ~80%, haze ~14%), moderate hydrophilic surface (contact angle ~71°) supporting adhesion for live coatings, safe according to the heavy metal–microbiological profile, and rapid biodegradation in compost. These results are consistent with the current understanding of Ca^{2+} immobilized pectin/protein hybrid films, reinforcing the potential for implementation as edible coatings for the fresh food supply chain.

Table 1 Safety indicators of the LMA–BBP film

Parameters	Units	Results	SD
Pb	mg kg^{-1}	0.05	0.00074
Cd	mg kg^{-1}	0.008	0.00006
As	mg kg^{-1}	0.02	0.00038
Hg	mg kg^{-1}	0.004	0.00002
TPC	CFU g^{-1}	<10	
Yeast & mold	CFU g^{-1}	<10	
E. coli (1 g)	CFU g^{-1}	Not detected	
Salmonella (25 g)	CFU g^{-1}	Not detected	
S. aureus (1 g)	CFU g^{-1}	Not detected	

3.6. Practical applications of preservative films

Field data on tomatoes and beef showed that the LMA–BBP coatings provided significantly better preservation performance than the pectin-only coating (PMA-only) and the control batch. In tomatoes (Fig. 9), the LMA–BBP coatings reduced weight loss and retained firmness the best compared to the other two batches; at the same time, TPC and spoilage rate were significantly lower over 12 days. This is a typical consequence of coating fruit with pectin films with a good oxygen barrier: respiration rates and ethylene production are lowered, ripening/softening is delayed, and transepidermal water loss is reduced; the protein component of the hybrid network regulates gas permeability at moderate RH, enhancing the microatmosphere packaging effect around the fruit surface. Review/test systems on tomatoes showed that edible coatings generally reduced mass loss (0.4–16%), retained firmness ~20–25% better, and reduced microbial contamination.[63,64]

In beef (Fig. 10), drip loss increased the slowest with LMA–BBP, indicating better water retention on the meat surface; the mechanism is consistent with the pectin network immobilizing Ca^{2+} and the protein phase forming a tight matrix, resulting in

a longer water vapor diffusion path and limiting moisture migration from muscle tissue to the environment, a trend that has been described for plasticized polysaccharide/protein films in reviews of moisture–gas barriers of edible films. At the same time, TPC increased the slowest with LMA–BBP; the graph shows that the commonly used spoilage threshold in fresh meat (~7 log CFU g^{-1}) was delayed compared to the control, consistent with recommendations/observations that 7 log CFU g^{-1} is the microbiological end-of-life for refrigerated red meat (according to MLA/ICMSF and many fresh meat studies). This is explained by the good oxygen barrier of the pectin matrix at moderate humidity, which, combined with the gas barrier of the protein layer, slows down microbial respiration and surface lipid oxidation. The TBARS (mg MDA per kg) increase was the slowest in the LMA–BBP sample, typical of a low OTR system: when less O_2 reaches the meat surface, lipid peroxidation chain reactions are inhibited. The increase in meat pH during storage (associated with the accumulation of volatile amines and degradation products) was also inhibited by LMA–BBP, consistent with reports that gas/moisture barrier coatings reduce the rate of pH change and microbial load in fresh meat. In addition to the barrier mechanism, insect proteins have been reported to
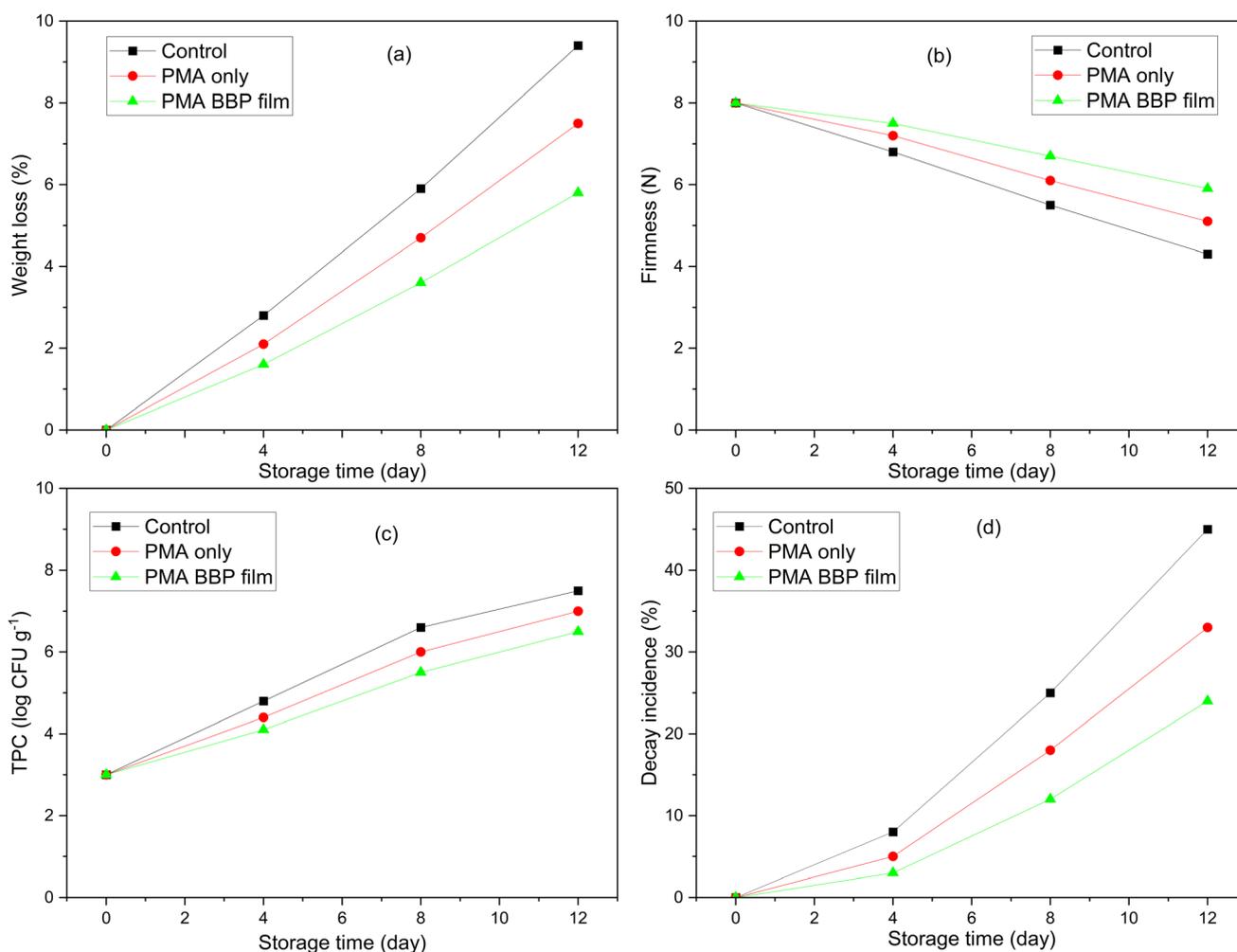

Fig. 9 Changes in parameters of tomato during storage using preservation films: weight loss (a); firmness (b); TPC (c) and decay incidence (d).
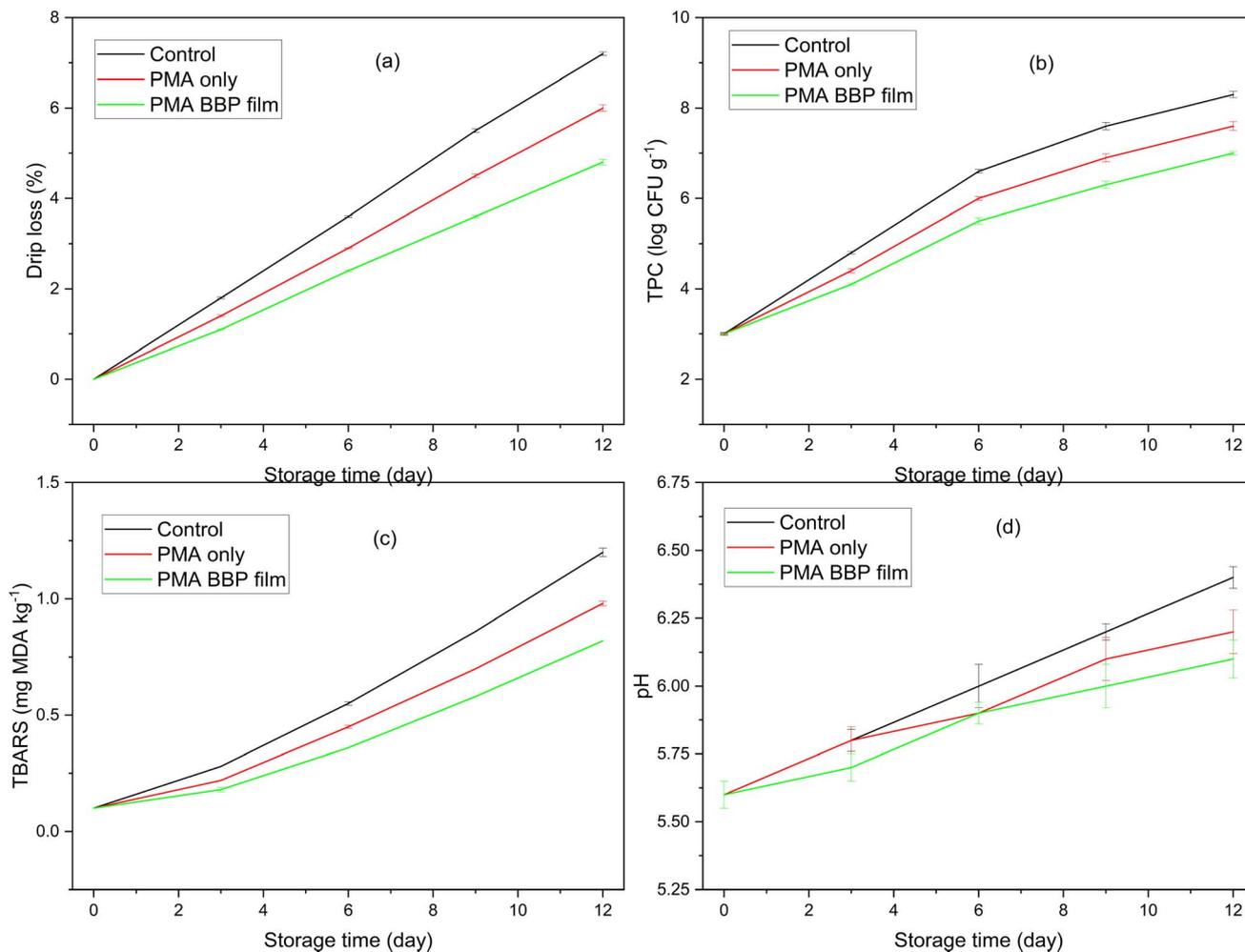
Fig. 10 Changes in parameters of beef during storage using preservative films: drip loss (a); TPC (b); TBARS (c) and pH (d).

contain potential antimicrobial/antioxidant peptides; BBP in the pectin–Ca^{2+} network may contribute to creating a less favorable surface environment for positively charged bacteria and reduce oxidative stress, an effect that has been noted in reviews of insect peptides and bioactive edible proteins/films.[65]

From a structure–function perspective, the superiority of LMA–BBP over PMA-only stems from two network layers: (i) pectin LM/LMA–Ca^{2+} forms egg-box-like junction zones that densify the matrix and reduce free volume; (ii) positively charged protein coacervation (coacervation at optimal pH) forms electrostatic/ion-pair bonds with –COO$^-$ of pectin, increasing the effective network density, thereby reducing OTR, adjusting WVP, and raising TS/E' while maintaining a useful EAB, a description consistent with polyelectrolyte coacervation theory and recent pectin–protein mixture studies. These mechanisms also explain the FTIR/UV-Vis/TGA-DSC patterns of the materials: Ca^{2+}/amide–COO$^-$ coordination traces, the 205/280 nm protein peak combination, and the pyrolytic/moisture–glycerol steps of the hybrid network.[47] Regarding safety, the film meets the physicochemical–microbiological criteria well: heavy metals at trace levels (Pb 0.05; Cd 0.008; As 0.02; Hg 0.004 mg kg^{-1}) and very low background microbiology (TPC, yeast–mold

<10 CFU g^{-1}; *E. coli*, *Salmonella*, *S. aureus*: not detected), consistent with the general safety picture of pectin (E440) which is considered by EFSA to have no safety concerns within the scope of use as a food additive/ingredient; many insect proteins also contain natural antimicrobial peptides, suggesting room for improving anti-spoiling properties when optimizing formulations.[66] In summary, beef (drip loss, TPC, TBARS, pH) and tomato (weight, firmness, TPC, rot percentage) performance parameters were consistently improved with the LMA–BBP layer compared to the pectin film alone and the control. This is consistent with current knowledge that pectin films are excellent oxygen barriers for fresh produce, while protein films have strong gas barriers at moderate humidity; the coacervation/egg-box combination creates a hybrid network that is both airtight and flexible enough to extend the microbiologically acceptable shelf life (approaching or exceeding the 7 log CFU g^{-1} threshold later), while reducing lipid oxidation and maintaining sensory/texture qualities throughout cold storage.

The proposed LMA–BBP dual-network platform has clear scale-up potential because its unit operations rely on established food/biopolymer processing steps: aqueous dissolution

and pH adjustment for complexation, solution casting/coating, low-temperature drying, and short CaCl$_2$ post-treatment. The optimized formulation (LMA 2.5% w/v; BBP 0.5% w/v; glycerol 25% on polymer; CaCl$_2$ ~1.5% w/v; pH ~4.7) already targets a narrow but controllable operating window, which can be translated to pilot production using inline pH monitoring and controlled mixing/degassing to maintain consistent coacervate structure and coatability. Practical processing challenges at a larger scale are expected to include: (i) viscosity drift and foam formation during high-solids mixing (requiring controlled shear and vacuum deaeration), (ii) uniform drying without edge cracking or thickness gradients, and (iii) managing the CaCl$_2$ step (concentration, contact time, and optional rinsing) to prevent salt accumulation, excessive stiffness, or optical haze. In addition, raw-material variability (citrus peel pectin quality and insect protein composition) necessitates basic incoming QC (DE/DM, ash, protein content, and microbial indicators) to keep performance reproducible. The BBP extraction route (defatting → alkaline extraction → isoelectric precipitation) is scalable but should incorporate solvent recovery and neutralization of acid/alkali streams to reduce operating cost and environmental load. From a cost perspective, the approach is attractive because it valorizes low-cost by-products (citrus peel) and emerging biomass (bee brood), while using commodity reagents (citric acid/NaOH/CaCl$_2$/glycerol). The main cost drivers are energy for drying, ethanol/solvent handling in protein defatting, and wastewater treatment; these can be mitigated through heat integration and solvent recycling. In terms of industrial applicability, the most immediate route is as edible coatings for fresh produce and chilled meat, where the demonstrated reductions in weight/drip loss, microbial growth, and oxidation translate into shelf-life extension under typical cold-chain conditions. However, because insect proteins may pose allergenicity and labeling considerations, risk assessment and clear labeling are required for commercial deployment depending on local regulations and target consumers.

3.7. Extrapolated evidence from insect protein films

Recent results have shown that insect proteins have the potential to form viable films in solution casting, especially when combined with a mild plasticizer and/or chemical crosslinker, with adequate mechanical–barrier properties for food contact packaging and can provide active preservation functions (antioxidant, antimicrobial) (Table 2). For example, silkworm pupa protein films applied to cheddar cheese have improved oxidative and microbiological stability, demonstrating their effectiveness in high-fat food substrates, a more challenging context than fresh fruit, which only requires a moderate moisture–gas barrier. These results suggest the transferability of our BBP system, especially when the technological strategy (solution casting, glycerol plasticization, and post-casting treatment) is similar.[26] In addition, cricket protein films supplemented with plant-based antimicrobials demonstrated clear inhibition rings against *E. coli* and *S. aureus*, emphasizing that insect proteins are not only film material matrices but also carriers for active agents, a point that is

consistent with the expansion of the pectin–BBP system if additional natural antibacterial/antioxidant properties are required. Structurally, some insect protein–plant protein composites (*e.g.*, locust/SPI) showed homogeneous cross-sections on SEM and improved mechanical properties with the presence of crosslinkers, providing indirect evidence that protein–polymer (in our case, protein–pectin) interactions can be organized into stable networks when pH/ion conditions and post-treatments are appropriate.[27,67]

From a chemo-physical tuning perspective, studies on black soldier fly (BSF) proteins show that mild crosslinking significantly improves tensile strength, while uncrosslinked films show poorer mechanical properties, a result that closely matches the mechanism of our system: Ca^{2+} forms an "egg-box" in pectin LM/LMA (reinforcing the polysaccharide network) while binding/modulation in the protein phase (if applicable) optimizes the TS–EAB–barrier equilibrium. Thus, in principle, the two structural levers, pectin–BBP electrophilic coacervation at pH near the protein pI and Ca^{2+} ion crosslinking, are supported by published observations in insect protein films in general.[68] Systematic reviews of insect-derived packaging materials note that insect protein films can achieve useful light transmission, mechanical–barrier properties by optimizing plasticizer, ionic/chemical bonding, and pH/ionic conditions; and post-processing recommendations (heat/pressure/enzymes) to enhance solubility-film-forming ability are recommended, recommendations that coincide with those used for BBP (defatting, alkaline extraction–isoelectric precipitation, pH adjustment blending, post-molding CaCl$_2$). On the other hand, the overview of protein-based films (not limited to insects) also concluded that proteins are good material bases for films/packaging, with the technological bottlenecks still being plasticization (glycerol/sorbitol), interaction promotion (ionic/enzymatic/mild chemical) and moisture–heat control.[69]

At the techno-functional level, many publications on mealworm, cricket, and BSF describe good foaming/emulsifying and interfacial stability, reflecting the active surface of insect proteins; this is the basis for homogenizing the polymer phase in the film when combined with negatively charged polysaccharides such as pectin LM/LMA. Regarding the charge–isoelectric point, studies have also shown that the net charge of insect proteins is pH-dependent, which is favorable for adjusting the coacervation window with pectin. These properties reinforce the universality of the positive protein–negative pectin hybrid network mechanism, which is not rigidly dependent on the specific insect species.[70] In addition, protein modifications by high pressure (HHP), polyphenol attachment, or amidation/enzymes have been shown to improve the solubility, intra-network interactions, and/or bioactivity of insect proteins. For example, HHP with mealworm improves the structure–function properties; gallic acid-bound silkworm pupae protein (on chitosan system) enhances the antioxidant properties, suggesting the possibility of inserting polyphenols into our system to enhance lipid protection (as seen in the cheese model). This opens the way for upgraded versions of pectin–BBP films (active/antimicrobial and antioxidant films) if the application needs to be extended beyond the foundation.[71,72]

Table 2 Some food preservation films from different materials

Materials	Core process	Key baseline properties	Food application target	Preservation effectiveness	Sources
Orange peel pectin (LM/LMA) + honeybee pupae protein (BBP) + CaCl$_2$	Aqueous solution casting; blend pH ~4.85; CaCl$_2$ dip 1.5% (90 s); glycerol 25% (on polymer)	TS 51 MPa; EAB 20.5%; WVP 4.6 g mm per m^2 per day per kPa; OTR 60 cm^3 per m^2 per day; thickness ~70 μm	Tomato (12 °C), beef (4 °C)	Shelf-life ↑ to ~12 days vs. ~8–9 days control; ↓ weight/drip loss; ↓ TPC; ↓ TBARS/TVB-N	This study
Silkworm pupae protein film + Catharanthus roseus leaf extract nanoparticles	Solution-cast protein film containing bioactive nanoparticles; applied to cheddar cheese	NR	Cheddar cheese (4–10 °C)	↓ Lipid oxidation (PV/TBARS), ↓ microbial growth; improved storage stability	26
Cricket (Acheta domesticus) protein film + Caralluma fimbriata extract nanoparticles	Bioactive protein film via solution casting; antimicrobial assessment	NR	Cheddar cheese/meat emulsion (model)	Clear inhibition vs. E. coli and S. aureus; potential shelf-life gains	27
Grasshopper protein (GP)/soy protein isolate (SPI) + xylose (crosslinker) + cinnamaldehyde	Solution casting; mild crosslinking + antimicrobial agent	Homogeneous cross-section (SEM); improved mechanical/ barrier (qualitative)	Antimicrobial packaging (material model)	Antimicrobial activity demonstrated; design cues for insect-protein composites	67
Black soldier fly (Hermetia illucens) prepupae protein films	Film casting; effect of protein solubility and mild crosslinking	TS ↑ with mild crosslinking; non-crosslinked films weaker (qualitative)	Bio-based packaging (material model)	(Material-focused; no direct food test)	68
Whey protein isolate (WPI) films with antimicrobials	Solution casting; sometimes with essential oils/nisin	TS typically 30–60 MPa; thickness 50–100 μm (range from reviews)	Fresh beef/red meat	Reduced spoilage flora; extended beef shelf-life depending on actives	73
Sodium alginate coating + cinnamon essential oil nanoparticles + nisin	Surface coating; Ca^{2+} gelation; refrigerated beef slices	NR	Beef slices	Shelf-life extended to ~15 days; ↓ weight loss; improved color/odor/ texture; ↓ microbes	74
Alginate–agar coating containing ginger essential oil (GEO)	Surface coating; refrigerated beef	NR	Beef	Shelf-life +3 to +9 days vs. control (dose-dependent); improved quality indices	75
Chitosan (2%) + cinnamon oil coating (CS–CO)	Surface coating; ambient tomato storage	NR	Tomato (ambient)	Extended shelf-life up to 14 days (<6.78 log CFU mL^{-1}); better physicochemical quality	76
Pectin (≈5%) single coating	Surface coating; mild drying	NR	Tomato	Shelf-life 9 → 11 days; ↓ weight loss; maintained biochemical quality	77

From a comparative perspective, Table 2 indicates that the optimized LMA–BBP–Ca^{2+} film reaches a balanced mechanical–barrier set (TS $\approx$ 51 MPa, OTR $\approx$ 60 cm^3 per m^2 per day, practical thickness ~70 µm) while being validated on two fresh-food matrices (tomato and beef) with consistent preservation gains. By comparison, representative insect-protein films summarized in Table 2 (e.g., silkworm or cricket protein films) are mainly demonstrated in cheese systems or as antimicrobial material models, and typically emphasize active-additive integration rather than an ionically reinforced polysaccharide scaffold. Likewise, pectin-only coatings can extend tomato shelf life but often with more modest increments than the dual-network hybrid. Therefore, the novelty of this study is not simply another pectin–protein blend, but a pectin–insect-protein dual-network platform (coacervation + Ca^{2+} egg-box) with cross-commodity relevance (produce and meat) and a mechanistically guided formulation pathway.

Novelty positioning relative to pectin–protein and insect-protein edible films. Existing pectin–protein film literature has largely established charge-driven complexation/coacervation as a route to densify the biopolymer network (often benchmarked in conventional protein systems such as whey/pectin or gelatin/pectin), where pH/ionic strength and charge balance dictate aggregation and final film compactness. In parallel, insect-protein edible films reported to date are typically protein–matrix films that rely on plasticization and mild crosslinking or incorporation of active additives to reach usable strength and functionality (Table 2). In contrast, the present work is distinct in both material choice and network design: it valorizes Hàm Yên orange peel LM/LMA pectin and bee brood protein (BBP, *Apis mellifera*) and implements a dual-structuring strategy: (i) complex coacervation between pectin($-$) and BBP($+$) near pH 4.7 to form a polymer-rich electrostatic network, coupled with (ii) post-casting Ca^{2+} "egg-box" cross-linking that locks homogalacturonan junction zones. This dual-network route integrates two orthogonal strengthening mechanisms within an aqueous casting workflow and is guided by a design–make–measure mapping of turbidity/ζ-potential/DLS to locate the coacervation window.

4 Conclusion

This study demonstrates a dual structural strategy for edible film materials from Ham Yen orange peel pectin LMA and bee pupal protein (BBP): electrostatic co-precipitation (complex coacervation, *i.e.*, without applied electric field/current) at pH 4.7, combined with egg-box Ca^{2+} densification on homo-galacturonan segments. At the optimal formulation (mid-level glycerol; CaCl$_2$ treatment ~1.5% w/v), the LMA–BBP film achieved a balanced performance profile including strength–flexibility (TS $\approx$ 51 MPa; EAB $\approx$ 20.5%; DMA E' $\approx$ 1.18 GPa), gas/moisture barrier at the level used for fresh coatings (OTR $\approx$ 60 cm^3 per m^2 per day; WVP $\approx$ 4.6 g mm per m^2 day per kPa), suitable optics (T_{600} $\approx$ 80%; haze $\approx$ 14%), and moderate hydrophilic surface (θ $\approx$ 71°) for adhesion to moist substrates. FTIR recorded Ca–pectinate coordination signals and amide–COO$^-$ interactions, SEM showed a tight cross-section with few

defects, TGA/DSC showed typical moisture loss–plasticization–degradation stages of ion-reinforced pectin networks, and UV-Vis reflected the characteristic combination of pectin and protein. Regarding safety, the Pb/Cd/As/Hg content was at trace levels, TPC/yeast–mold microbial background <10 CFU g^{-1} and no *E. coli*, *Salmonella*, *S. aureus* were detected; regarding the environment, the material degraded rapidly under laboratory composting conditions (~18% of the remaining mass on day 60). Field storage tests on beef (4 °C) and tomatoes (12 °C) showed that the LMA–BBP coating reduced liquid/weight loss, inhibited TPC increase, delayed lipid oxidation (TBARS), and retained firmness, and had better pH stability than the control and single pectin films, consistent with the oxygen barrier mechanism of pectin, gas barrier of the protein phase, and increased network density due to Ca^{2+}. Overall, the LMA–BBP system showed high transferability: locally available raw materials, simple extraction–deposition process, suitable properties for fresh packaging, favorable safety-environment profile; the above optimization directions are the basis for bringing the material to industrial applications and expanding to functional coatings for many food chains.

Author contributions

Y. Doan Trang Tran: writing – original draft, conceptualization, methodology, data curation, formal analysis. Thi Thao Minh: writing – original draft, data curation, formal analysis. Dinh Nhi Bui: writing – original draft, conceptualization, methodology, writing – review & editing, and supervision. Thi Dung Ha: data curation, formal analysis, conceptualization, methodology, writing – review & editing.

Conflicts of interest

The authors declare that they have no known competing financial interests or personal relationships that could have appeared to influence the work reported in this paper.

Data availability

Data will be made available on request.

Acknowledgements

References

1 A. Syarifuddin, M. H. Muflih, N. Izzah, U. Fadillah, A. F. Ainani and A. Dirpan, *Carbohydr. Polym. Technol. Appl.*, 2025, **9**, 100680.

2 S. Suri, A. Singh and P. K. Nema, *Appl. Food Res.*, 2022, **2**, 100050.

3 C. Russo, A. Maugeri, G. E. Lombardo, L. Musumeci, D. Barreca, A. Rapisarda, S. Cirmi and M. Navarra, *Molecules*, 2021, **26**, 5991.

4 S. AlZahabi and W. Mamdouh, *RSC Adv.*, 2025, **15**, 36534–36595.

5 S. Kaur, V. Singh, P. Vern and P. S. Panesar, *Process Biochem.*, 2025, **158**, 81–98.

6 M. R. V. Bertolo, T. S. Pereira, F. V. dos Santos, M. H. M. Facure, F. dos Santos, K. B. R. Teodoro, L. A. Mercante and D. S. Correa, *Compr. Rev. Food Sci. Food Saf.*, 2025, **24**(2), e70144.

7 N. Medina-Herrera, G. C. G. Martínez-Ávila, C. L. Robledo-Jiménez, R. Rojas and B. S. Orozco-Zamora, *Biomass*, 2024, **4**, 784–808.

8 F. A. H. Prakoso, R. Indiarto and G. L. Utama, *Polymers*, 2023, **15**, 2800.

9 L. Cao, W. Lu, A. Mata, K. Nishinari and Y. Fang, *Carbohydr. Polym.*, 2020, **242**, 116389.

10 V. Chandel, D. Biswas, S. Roy, D. Vaidya, A. Verma and A. Gupta, *Foods*, 2022, **11**, 2683.

11 N. Riyamol, J. Gada Chengaiyan, S. S. Rana, F. Ahmad, S. Haque and E. Capanoglu, *ACS Omega*, 2023, **8**, 46309–46324.

12 M. J. Akhter, S. Sarkar, T. Sharmin and S. C. Mondal, *Appl. Food Res.*, 2024, **4**, 100614.

13 B. Akachat, L. Himed, M. Salah, M. D'Elia, S. Zomorroda, R. Ali, L. Rastrelli and M. Barkat, *Appl. Food Res.*, 2025, **5**, 100948.

14 C. Zheng, W. Huang, Y. Zou, W. Huang, G. Zhang and P. Fei, *Food Res. Int.*, 2022, **160**, 111719.

15 C. Zheng, Y. Zou, Y. Huang, B. Shen, P. Fei and G. Zhang, *Food Hydrocolloids*, 2023, **134**, 108037.

16 W. A. Asfaw, K. D. Tafa and N. Satheesh, *Heliyon*, 2023, **9**, e13724.

17 C. A. A. Amadeu, F. B. Silva, C. J. F. Souza, M. T. Koschevic, V. Schoeninger, E. A. Falcão, V. A. D. S. Garcia, C. A. L. Cardoso and S. M. Martelli, *Polymers*, 2024, **16**, 3158.

18 A. Archut, S. Drusch and H. Kastner, *Food Hydrocolloids*, 2022, **133**, 107884.

19 A. Archut, M. Klost, S. Drusch and H. Kastner, *Food Hydrocolloids*, 2023, **134**, 108032.

20 S. Im, O. G. Jones and S. J. Choi, *Foods*, 2023, **12**, 4217.

21 L. Fu, F. Ding, X. Huang and X. Zou, *Colloids Surf., B*, 2025, **256**, 115025.

22 J. Yang, W. Cai, M. Rizwan Khan, N. Ahmad, Z. Zhang, L. Meng and W. Zhang, *Foods*, 2023, **12**, 3336.

23 S. Roy and J.-W. Rhim, *Materials*, 2022, **15**, 3769.

24 R. P. F. Guiné, S. G. Florença, M. J. Barroca and C. A. Costa, *Insects*, 2025, **16**, 796.

25 F. Zhang, Q. Yue, X. Li, B. Kong, F. Sun, C. Cao, H. Zhang and Q. Liu, *Ultrason. Sonochem.*, 2023, **94**, 106335.

26 S. Noor, S. Kumar, H. F. Bhat, A. Hassoun, R. M. Aadil, S. A. Khandi, M. S. Azad, G. Abdi and Z. F. Bhat, *Food Hydrocolloids Health*, 2024, **6**, 100183.

27 A. B. Lone, H. F. Bhat, S. Kumar, A. Aït-Kaddour, R. M. Aadil, A. Hassoun and Z. F. Bhat, *Ultrason. Sonochem.*, 2025, **112**, 107167.

28 L. De Marchi, A. Wangorsch and G. Zoccatelli, *Curr. Allergy Asthma Rep.*, 2021, **21**, 35.

29 J. Yang, S. Zhou, H. Kuang, C. Tang and J. Song, *Crit. Rev. Food Sci. Nutr.*, 2024, **64**, 10361–10383.

30 F. Coin, A. Larrañaga and S. Cerveny, *Carbohydr. Polym. Technol. Appl.*, 2025, **11**, 100885.

31 V. Souza, I. Mello, O. Khalid, J. Pires, C. Rodrigues, M. Alves, C. Santos, A. Fernando and I. Coelhoso, *Coatings*, 2022, **12**, 108.

32 N. S. Said, I. F. Olawuyi and W. Y. Lee, *Polymers*, 2024, **16**, 712.

33 H. Guo, J. Bai, X. Jin, H. Liu, D. Wu, R. Gan and H. Gao, *LWT*, 2024, **214**, 117102.

34 L. Castillo-Rodríguez, A.-S. Hernández-Cázares, M. Rojas-López, J.-V. Hidalgo-Contreras, A. López-Malo and M.-A. Rios-Corripio, *CyTA J. Food*, 2025, **23**(1), 2525175.

35 S. Singhal and N. R. Swami Hulle, *Appl. Food Res.*, 2022, **2**, 100215.

36 C. Zheng, Z. Zhang, N. Ding, B. Huang, G. Zhang and P. Fei, *Food Hydrocolloids*, 2022, **125**, 107454.

37 J. Pan, H. Xu, Y. Cheng, B. Mintah, M. Dabbour, F. Yang, W. Chen, Z. Zhang, C. Dai, R. He and H. Ma, *Foods*, 2022, **11**, 2931.

38 B. Zozo, M. Wicht and J. van Wyk, *Appl. Sci.*, 2024, **14**, 11485.

39 M. Mishyna, J. K. Keppler and J. Chen, *Curr. Opin. Colloid Interface Sci.*, 2021, **56**, 101508.

40 M. Hoque, R. P. Babu, C. McDonagh, S. Jaiswal, B. K. Tiwari, J. P. Kerry and S. Pathania, *Int. J. Biol. Macromol.*, 2024, **271**, 132414.

41 E. Basiak, A. Lenart and F. Debeaufort, *Polymers*, 2018, **10**, 412.

42 S. Guzman-Puyol, J. J. Benítez and J. A. Heredia-Guerrero, *Food Res. Int.*, 2022, **161**, 111792.

43 A. Botalo, T. Inprasit, S. Ummartyotin, K. Chainok, S. Vatthanakul and P. Pisitsak, *Polymers*, 2024, **16**, 447.

44 S. Drusch, M. Eichhorn, S. Heinert, J. Weißbrodt and R. Morales-Medina, *Food Hydrocolloids*, 2024, **156**, 110289.

45 X. Wan, M. Zhao, M. Guo, P. Li, H. Shi, X. Zhang, Z. Liu and G. Xia, *Food Chem.: X*, 2023, **18**, 100703.

46 L. Li, B. Lai, J.-N. Yan, M. H. Yambazi, C. Wang and H.-T. Wu, *Food Hydrocolloids*, 2024, **148**, 109445.

47 M. Alrosan, N. Al-Rabadi, M. H. Alu'datt, A. Al-Qaisi, E. E. Al-Shunnaq, N. Abu-Khalaf, S. Maghaydah, T. Assaf, T. Hidmi, T.-C. Tan, H. Bawadi, A. M. Almajwal and H. J. Obeidat, *Food Eng. Rev.*, 2025, **17**, 1059–1082.

48 D. E. Igartúa, D. M. Cabezas and G. G. Palazolo, *Food Chem. Adv.*, 2022, **1**, 100123.

49 Ş. Ürüncüoğlu, K. Alba, G. A. Morris and V. Kontogiorgos, *Curr. Res. Food Sci.*, 2021, **4**, 398–404.

50 I. Fraeye, T. Duvetter, E. Doungla, A. Van Loey and M. Hendrickx, *Trends Food Sci. Technol.*, 2010, **21**, 219–228.

51 A. S. Giz, M. Berberoglu, S. Bener, S. Aydelik-Ayazoglu, H. Bayraktar, B. E. Alaca and H. Catalgil-Giz, *Int. J. Biol. Macromol.*, 2020, **148**, 49–55.

52 H. Wei and M. A. Pascall, *Polym. Eng. Sci.*, 2023, **63**, 2522–2533.

53 M. M. Saldívar Guevara, V. Saucedo-Rivalcoba, J. L. Rivera-Armenta and L. I. Elvira Torales, *Cellul. Chem. Technol.*, 2022, **56**, 1061–1070.

54 Z. Eslami, S. Elkoun, M. Robert and K. Adjallé, *Molecules*, 2023, **28**, 6637.

55 A. A. B. A. Mohammed, Z. Hasan, A. A. B. Omran, A. M. Elfaghi, M. A. Khattak, R. A. Ilyas and S. M. Sapuan, *Polymers*, 2022, **15**, 63.

56 M. Schmid, *Materials*, 2013, **6**, 3254–3269.

57 T. Chuenkaek and T. Kobayashi, *ACS Sustainable Resour. Manage.*, 2024, **1**, 213–224.

58 H. Xue, L. Ji, K. Zhang, P. Wang, X. Liao and J. Tan, *J. Future Foods*, 2025, DOI: 10.1016/j.jfutfo.2025.05.011.

59 I. Obomighie, I. J. Prentice, P. Lewin-Jones, F. Bachtiger, N. Ramsay, C. Kishi-Itakura, M. W. Goldberg, T. J. Hawkins, J. E. Sprittles, H. Knight and G. C. Sosso, *Commun. Biol.*, 2025, **8**, 72.

60 A. Fernandez-Prior, L. Barrera-Chamorro, E. Marquez-Paradas, C. López-de-Dicastillo, M. C. Millan-Linares, A. Villanueva-Lazo and S. Montserrat-de la Paz, *J. Sci. Food Agric.*, 2025, **105**, 5863–5873.

61 W. Bai, N. P. Vidal, L. Roman, G. Portillo-Perez and M. M. Martinez, *Int. J. Biol. Macromol.*, 2023, **251**, 126383.

62 D. G. M. Pereira, J. M. Vieira, A. A. Vicente and R. M. S. Cruz, *Polymers*, 2021, **13**, 2632.

63 N. S. Said and W. Y. Lee, *Molecules*, 2025, **30**, 1144.

64 H. T. Duguma, *Int. J. Food Sci. Technol.*, 2022, **57**, 1353–1366.

65 M. N. Khin, S. Ahammed, Md. M. Kamal, M. N. Saqib, F. Liu and F. Zhong, *Food Hydrocolloids Health*, 2024, **6**, 100182.

66 M. Li, C. Mao, X. Li, L. Jiang, W. Zhang, M. Li, H. Liu, Y. Fang, S. Liu, G. Yang and X. Hou, *Foods*, 2023, **12**, 4073.

67 Z. Zhang, X. Zhou, C. Fang and D. Wang, *Front. Nutr.*, 2022, **9**, 796356.

68 D. Nuvoli, G. Montevecchi, F. Lovato, F. Masino, M. Van Der Borght, M. Messori and A. Antonelli, *J. Sci. Food Agric.*, 2021, **101**, 4506–4513.

69 S. Weng, I. Marcet, M. Rendueles and M. Díaz, *Food Packag. Shelf Life*, 2023, **38**, 101097.

70 L. S. Queiroz, N. F. Nogueira Silva, F. Jessen, M. A. Mohammadifar, R. Stephani, A. Fernandes de Carvalho, Í. T. Perrone and F. Casanova, *Heliyon*, 2023, **9**, e14831.

71 K. G. Zinoviadou, K. P. Koutsoumanis and C. G. Biliaderis, *Food Hydrocolloids*, 2010, **24**, 49–59.

72 M. Zhang, W. Luo, K. Yang and C. Li, *J. Food Prot.*, 2022, **85**, 896–905.

73 B. Zhang, Y. Liu, H. Wang, W. Liu, K. Cheong and B. Teng, *Food Control*, 2021, **130**, 108216.

74 K. Venkatachalam, S. Lekjing, P. Noonim and N. Charoenphun, *Foods*, 2024, **13**, 1000.

75 G. K. Jhanani, M. S. AlSalhi, N. T and R. Shanmuganathan, *Environ. Res.*, 2024, **258**, 119368.

76 A. Boukil, A. Marciniak, S. Mezdour, Y. Pouliot and A. Doyen, *Foods*, 2022, **11**, 956.

77 K. Yi, B. Yang, Y. Wu, S. Miao and Y. Lu, *Foods*, 2025, **14**, 3280.